Deciphering the specific interaction between the acyl carrier protein IacP and the T3SS-major hydrophobic translocator SipB from *Salmonella*

Mickaël J. Canestrari[a], Bastien Serrano[a], Julia Bartoli[a], Valérie Prima[a], Olivier Bornet[b], Rémy Puppo[c], Emmanuelle Bouveret[a,*], Françoise Guerlesquin[a], and Julie P. Viala[a,#]

[a] LISM, Institut de Microbiologie de la Méditerranée, CNRS and Aix-Marseille Univ., Marseille, France

[b] NMR Platform, Institut de Microbiologie de la Méditerranée, CNRS and Aix-Marseille Univ., Marseille, France

[c] Proteomics Platform- IBISA[2], Institut de Microbiologie de la Méditerranée, CNRS and Aix-Marseille Univ., Marseille, France

Running head: T3SS-associated acyl carrier proteins

#Address correspondence to Julie P. Viala: jviala@imm.cnrs.fr

*Present address: SAMe Unit, Microbiology Department, Pasteur Institute, Paris, France

Keywords: acyl carrier protein, type 3 secretion system, translocon, translocator, protein-protein interaction, acylation, *Salmonella*, SPI 1, IacP, SipB, ACP

Abbreviations used: SPI-1, *Salmonella* pathogenicity island 1; T3SS, type 3 secretion system; 4'-PP, 4'-phosphopantetheine; HSQC, heteronuclear single quantum coherence; pfe, *Pseudomonas fluorescens*; sfl, *Shigella flexneri*; stm, *Salmonella* Typhimurium

ABSTRACT

Salmonella is a facultative intracellular pathogen that invades epithelial cells of the intestine using the SPI-1 Type 3 secretion System (T3SS). Insertion of the SPI-1 T3SS translocon is facilitated by acylation of the translocator SipB, which involves a protein-protein interaction with the acyl carrier protein IacP. Using nuclear magnetic resonance and biological tests we identified the residues of IacP that were involved in the interaction with SipB. Our results suggest that the 4'-phosphopantethein group that functionalizes IacP would participate to the interaction. Its solvent exposition might rely on two residues highly conserved in acyl carrier proteins associated with T3SS. This study is the first to address the specificity of acyl carrier proteins associated with T3SS.

INTRODUCTION

Salmonella enterica serovar Typhimurium (*S.* Typhimurium) is a Gram-negative bacterium and facultative intracellular pathogen contracted by ingestion of contaminated food or water. Infection with *S.* Typhimurium typically results in a self-limiting diarrheal disease. During infection, *S.* Typhimurium relies on two Type 3 Secretion Systems (T3SS). Entry into epithelial cells is mediated by the T3SS encoded by *Salmonella* pathogenicity island 1 (SPI-1) and intracellular proliferation is promoted by the T3SS encoded by SPI-2 [1]. T3SSs are a molecular syringe-like machinery that inject effector proteins directly from bacteria into the host-cell cytosol. Perforation of the host plasma membrane is mediated by a translocon located at the apex of the T3SS needle. The SPI-1 T3SS translocon is formed by the hydrophilic translocator SipD (SctA in the unified nomenclature for T3SS components), also called the "needle tip protein", as well as the minor hydrophobic translocator SipC (SctB in the unified nomenclature for T3SS components) and the major hydrophobic translocator SipB (SctE in the unified nomenclature for T3SS components) [2–4]. Both SipB and SipC contain transmembrane segments and the SipB-SipC complex is essential for the formation of the translocon [2, 5]. However, the exact organization of the translocon is still unknown. In addition, although the structures of the needle and tip proteins have been solved, determining the structures of the translocators has met with little success. Only the structure of a soluble N-terminal region of SipB, representing a quarter of the protein (residues 82 to 226), has been solved and is organized as a trimeric coiled-coil [6]. Premature association of SipB and SipC is prevented in the bacterial cytosol by their respective association with the chaperone SicA. In the absence of SicA, translocators tend to be degraded [7]. SicA binds within the 100 N-terminal residues of SipB [8–10]. SipB and SipC separate from their chaperon when the time

comes for secretion through the T3SS. Recently, we showed that prior to secretion, SipB is acylated on the side chain of its unique cysteine residue. This posttranslational modification requires the intervention of a specific acyl carrier protein, called IacP, for invasion acyl carrier protein, which is also encoded by SPI-1. A protein-protein interaction between IacP and SipB has been demonstrated to take place in the bacterial cytosol, and the subsequent acylation of SipB optimizes its insertion into host membranes [11]. However, the exact purpose of this acylation and when it becomes truly beneficial for pathogenesis is still unknown.

Acyl carrier proteins are cofactors of primary and secondary metabolic pathways that carry and present a nascent metabolite to the appropriate enzymes [12, 13]. They are small proteins of approximately 80 residues that are generally organized as four -helix bundles, hence delimitating an internal hydrophobic pocket into which the substrate is sequestered. Acyl carrier proteins are synthesized as apo-proteins that require the addition of a 4'-phosphopantetheine prosthetic group (4'-PP) to be functional (holo-proteins). Indeed, 4'-PP constitutes a flexible arm of 18 Å, at the extremity of which a sulfhydryl group allows attachment of the nascent metabolite with a thioester bond. The 4'-PP group is linked to the side chain of a conserved serine residue that belongs to a Pfam PP-binding motif [14]. Among acyl carrier proteins, ACP, encoded by the gene *acpP*, is the essential cofactor of fatty acid synthesis and the most studied member of this protein family. ACP shuttles the elongating fatty acid to each enzyme of the biosynthetic pathway. Once the fatty acid has reached a length of 16 to 18 carbons, it is delivered to acyltransferases of the phospholipid biosynthetic pathway. In Gram-negative bacteria, ACP also provides substrates to acyltransferases of the lipopolysaccharide (LPS) biosynthetic pathway. In addition, fatty acids carried by ACP are also used for the synthesis of biotin and lipoic acid [15] and to acylate proteins of the RTX-toxin family in certain Gram-negative pathogens [16]. Hence, ACP is a constitutively

produced and abundant protein which has numerous protein partners [13, 17, 18]. There is no common ACP-binding motif identified among the partner enzymes. However, an interaction between ACP and a partner protein often involves the anionic -helix 2 of ACP and a basic/ hydrophobic patch near the active site of the partner enzyme.

In *Salmonella*, although ACP also has the ability to bind to many proteins, it does not interact with the major hydrophobic translocator SipB [11]. Our aim was to identify the intrinsic determinants of IacP, the acyl carrier protein associated with SPI-1 T3SS, that allow its specific interaction with SipB. This study contributes to the characterization of this type of acyl carrier protein, which is associated with T3SS and therefore bacteria-host interactions, and which has been little studied to date.

MATERIALS AND METHODS

Bacterial strains and growth conditions

E. coli and *S.* Typhimurium strains used in this study are described in Table 3. Bacteria were grown in 2YT, Luria-Bertani (LB) (Sigma-Aldrich), Brain Heart Infusion (Becton Dickinson), and M9 minimal medium (1X M9 salts, 1 mM $MgSO_4$, 0.1 mM $CaCl_2$, 0.5 µg/ml, 0.2% glucose). Antibiotic-based selection was performed with ampicillin (100 µg/ml) and kanamycin (25 to 50 µg/ml).

DNA manipulation

Plasmids used or created for this study are described in Table S1. PCR amplifications were performed with Phusion High-Fidelity DNA Polymerase (Finnzymes) and the bacterial genomes used as templates were from *S.* Typhimurium 12023, *S. flexneri* M90T, and *P. fluorescens* F113. Site-directed mutagenesis was performed on plasmids following the instructions of the QuickChange site-directed mutagenesis kit (Stratagene). Primers used for cloning and mutagenesis are listed in Table S2.

Bacterial two-hybrid system

We used the bacterial adenylate cyclase-based two-hybrid system to follow protein-protein interactions [19]. Pairs of proteins to be tested were fused to the C-terminal side of the two catalytic domains, T18 and T25, of adenylate cyclase using the plasmids pUT18Clink and

pKT25link [20]. *E. coli* BTH101 were co-transformed with the constructs corresponding to the hybrid-protein pairs to be tested and the co-transformants grown for two days at 30°C. Selection and subsequent growth of the co-transformants were performed on media containing ampicillin and kanamycin. One milliliter of LB medium, containing 0.5 mM IPTG (Isopropyl ß-D-thiogalactopyranoside), was inoculated with co-transformants and grown overnight at 30°C. ß-galactosidase activity was either visualized by spotting 2 µl of overnight cultures on LB plates, containing 0.5 mM IPTG and 40 µg/ml of the chromogenic substrate X-Gal (5-bromo-4-chloro-3-indolyl-β-D-galactopyranoside), or determined as previously described [21]. The values presented are the mean of three independent assays and the error bars represent the standard deviation.

Protein production and purification on cobalt beads

We produced the 6-histidine-tagged IacP and 6-histidine-tagged variants of IacP using the $pET_{6His\text{-}TEV}$ plasmid, which allows T7 promoter-driven production of a recombinant protein containing the N-terminal sequence, MGSSHHHHHHSSGRENLYFQGEF [22]. For protein production, *E. coli* BL21 (DE3) pLys were transformed with $pET_{6His\text{-}TEV}$ plasmids. Transformants were grown in LB at 35°C to $OD_{600} \approx 0.8$ and T7 promoter-driven production of the recombinant protein induced with 1 mM IPTG for 6 h at 30°C. A cytosolic protein extract was prepared and the 6-histidine-tagged proteins purified on cobalt beads as previously described [11]. A similar protocol was performed to obtain ^{15}N, ^{13}C labeled IacP for NMR assignment, except that when the bacterial culture reached $OD_{600} \approx 0.8$, bacterial

cells were washed twice and then resuspended in M9 minimal medium containing 1 g/L $^{15}NH_4Cl$ and 2 g/L $^{13}C_6$-glucose as the sole sources of nitrogen and carbon, respectively. Induction of the T7 promoter was then triggered with 1 mM IPTG and lasted overnight at 25°C. Similarly, to obtain ^{15}N labeled IacP and ^{15}N labeled IacP variants for HSQC experiments, bacterial cells were washed twice with 1X M9 salts, when the cultures reached $OD_{600} \approx 0.8$, and resuspended in M9 minimal medium containing 1g/L $^{15}NH_4Cl$. The sequential assignment of NH from 4'-PP was obtained by specific labeling using M9 medium supplemented with 1 g/L labeled ^{15}N aspartate and various concentrations of non-labeled amino acids based on the study of Vourtsis *et al*., 2014 [23].

The production of 6-histidine-tagged SipB (from pJV85) and 6-histidine-tagged SicA (from pJV101) was driven by the tetracycline-inducible promoter of the pP_{TET} plasmid. *E. coli* MG1655 was transformed with the constructed plasmids and the production and purification steps performed as previously published [11], except that the detergent NP-40 was removed from the purification buffers to co-purify SipB and its chaperon, both co-expressed from pJV85.

Mass-spectrometry analysis of intact proteins

Purified proteins were desalted for 24 h by dialysis into 20 mM ammonium bicarbonate pH 8. The protocol used for mass spectrometry analysis was slightly modified from that of Viala *et al*., 2013 [24]. Samples were treated according to the dry droplet method. Protein samples

(0.5 to 1 μL, corresponding to 25 to 75 pmol) were spotted onto a stainless-steel target plate with an equal volume of a saturated solution of α-cyano-4-hydroxy-cinnamic acid (70/30 acetonitrile/water 0.1% trifluoroacetic acid). Mixtures were allowed to dry at room temperature.

NMR spectroscopy experiments

All NMR experiments were recorded on IacP or IacP variants at 300K on a 600 MHz Bruker spectrometer equipped with a TCI cryoprobe. All NMR spectra were processed using TopSpin software from Bruker and analyzed using CARA [25]. The backbone sequential assignment of IacP was obtained by triple resonance heteronuclear experiments. HNCA, HNCOCA, HNCACB, CBCACONH, HNCO, and HNCACO spectra were recorded on a sample of ^{13}C, ^{15}N-labeled IacP at a concentration of 0.5 mM. For NMR experiments, protein samples were dialyzed against 20 mM sodium phosphate pH7, incubated for 48 h with 1 mM DTT, and 10% D_2O added before recording the spectra. Each NH cross-peak was assigned to one residue of the IacP sequence. ^{1}N-^{15}N HSQC of IacP variants were recorded under the same conditions (buffer and temperature). Because of the nature of the residues, the peak corresponding to the substituted residue disappears from the spectrum of the mutant protein and an additional peak, corresponding to the substituted alanine residue, appears in a different part of the spectrum. The spectrum is largely conserved for variants with correct folding, with minor changes corresponding to modification of the chemical environment of some NH groups due to the substitution. Large modifications are observed in the spectrum for variants with a major

structural change. Finally, peaks are observed at the center of the spectrum for unfolded variants (between 8.5 and 8.0 ppm).

For NMR titration of IacP/SipB complex formation, two independent series of ^{15}N-HSQC spectra were recorded for ^{15}N-labeled IacP at a concentration of 50 mM, in the presence of 0, 0.5, 1, 1.5, and 2 equivalents of the SipB /SicA complex (1:1), to obtain a soluble form of SipB. ^{15}N-HSQC spectra were recorded on ^{15}N-labeled IacP at a concentration of 50 mM in the presence of two equivalents of SicA to quantify the effect of the chaperon on the IacP NMR spectra. The resonances corresponding to residues affected during complex formation shifted in the spectrum with 0.5 equivalents of SipB and a strong decrease of intensity for these peaks was observed at higher SipB/SicA concentrations. These results indicate that the IacP/SipB complex is in a medium range exchange at the NMR time scale. We could not perform IacP spectra at higher SipB concentrations to obtain the NMR spectrum of the bound IacP, due to the low quantity of purified SipB.

Hemolysis assays

Hemolytic activity of *S.* Typhimurium SL1344 on sheep red blood cells (sRBC) was measured as previously described [11]. For bacterial strains transformed with the pP_{TET} plasmids, expression from the tetracycline promoter was triggered with 5 ng/ml anhydrotetracycline during bacterial growth and infection of sRBC.

Western Blots

Western blotting was performed on whole-cell extracts prepared from *E. coli* DH5α transformed with the pUT18Clink constructs and grown to $OD_{600} \approx 0.5$ before production of the hybrid protein was induced with 1 mM IPTG for 2 h. The CyaA antibody 3D1 (Santa Cruz Biotechnology) was used to detect the T18-hybrid proteins.

Complementation assay of E. coli ACP^{ts}

The *E. coli* ACP temperature-sensitive strain (ACP^{ts}) was transformed with the indicated plasmids used for the bacterial two-hybrid assays carrying a wildtype or mutated version of *acpP* fused to the T18 fragment of adenylate cyclase. Transformants were spread on LB plates containing ampicillin and incubated at 30 or 42°C for three days. Only strains able to complement the ACP temperature-sensitive phenotype could grow at 42°C.

RESULTS

Mapping of IacP residues that are involved in the interaction with SipB- We established the interacting residues on *S.* Typhimurium IacP by first using nuclear magnetic Resonance (NMR) to map the residues of IacP that are affected by interaction with SipB. A two-dimensional $^{1}H/^{15}N$-HSQC (heteronuclear single quantum coherence) spectrum was recorded for ^{15}N-labeled IacP (Fig. 1A). Peaks in this spectrum correspond to N/H correlations for the amide group of IacP residues. We obtained the sequential backbone assignment of the peaks according to the IacP sequence using a triple resonance (^{1}H, ^{15}N, ^{13}C) strategy (Fig. 1A). This spectrum represents the fingerprint of the protein at pH 7.0 and 300K after 48 h of incubation in 1 mM DTT. The chemical shift variations in this spectrum induced by a ligand interaction allow mapping of the interacting site on IacP. Thus, incubating ^{15}N-labeled IacP (Fig. 1B) with SipB should provide the interaction interface of SipB on IacP. We used a SicA/SipB complex because we previously observed that SicA was necessary to detect the interaction between IacP and SipB [11] and because this interaction normally occurs in the bacterial cytosol, where SipB is bound to SicA [7]. Thus, SipB was extracted as a soluble protein from the supernatant of cell extracts in the presence of SicA to perform NMR experiments (Fig. 1B).

Addition of the SipB/SicA complex induced chemical shift variations in the ^{15}N-labeled IacP spectrum (Fig. 1C). SicA alone had no effect on the IacP spectrum (Fig. 1D), indicating that the observed shifts reflect the interaction between SipB and IacP. Based on our IacP backbone

assignment (Fig. 1A), we could attribute the observed chemical shift perturbations to residues N25, G26, L30, V31, E32, D33, D37, S38, L39, L41, F46, G47, L48, S49, C56, L61, and F67 of IacP in the presence of the SicA/SipB complex. We recorded the IacP ^{15}N-HSQC spectra for different equivalents of the SipB/SicA complex (0, 0.5, 1, 1.5, and 2 equivalents) and observed that the NH cross-peaks corresponding to these residues first decreased in intensity and shifted (at 0.5 and 1 equivalent) and then disappeared at higher concentrations of the SipB/SicA complex (1.5 and 2.0 equivalents). As the other resonances of IacP were still observable, we concluded that these resonances were involved in the IacP/SipB complex interface and that the chemical exchange between the free and bound IacP occurred at an intermediate rate at the NMR time scale.

Determination of key IacP residues for the interaction with SipB- Next, we used a bacterial two-hybrid assay to examine the interaction between IacP and SipB. The bacterial two-hybrid system is based on the reconstitution of the *Bordetella Pertussis* adenylate cyclase activity by bringing together the T18 and T25 domains [26]. On the basis of the NMR chemical shift mapping, we made a series of point substitutions in IacP (N25A, G26A, L30A, V31A, E32A, D33A, D37A, S38T, L39A, L41T, F46A, G47A, L48A, S49A, C56A, L61A and F67A). The production of T18-IacP chimera proteins (wildtype and point mutants) was detected by western blotting (Fig. S1A). We systematically tested the interaction of SipB with each variant of IacP (Fig. 2). The L30A, V31A, E32A, D37A, S38T, L39A, L41T, L48A, and L61A substitutions altered the interaction between IacP and SipB (Fig. 2). We further characterized these variants by mass spectrometry to examine whether they were modified by the addition of 4'-PP (Table 1), and in a hemolytic assay to observe whether they also showed

a dysfunctional interaction with SipB in *S*. Typhimurium (Fig. 3).

Our previous data suggested that the addition of 4'-PP to IacP is essential to detect the interaction with SipB. Indeed, we showed that substitution of the conserved S38 residue prevents phosphopantetheinylation of IacP, as well as its interaction with SipB [11, 24]. Among the other point substitutions of IacP that we studied, only L39A prevented 4'-PP addition (Table 1). This mutant was unable to interact with SipB (Fig. 2), consistent with previous results. Consequently, we dropped variant L39 from the study and only variant S38T was kept as a negative control.

In addition to the bacterial two-hybrid test in *E. coli*, we measured hemolytic activity on sheep red blood cells (sRBCs) as a reporter assay of the interaction between IacP and SipB in *S*. Typhimurium. Indeed, the Δ*iacP S*. Typhimurium strain, in which the acylation of SipB is impaired, loses ~ 50% of its hemolytic activity relative to the wildtype strain (see Fig. 3, dashed line). Complementation with a wildtype version of IacP restores full hemolytic activity, contrary to the S38T variant, which is unable to interact with SipB ([11] and Fig. 3). The hemolytic activity observed above the dashed line in Fig. 3 thus reports the state of the interaction between IacP and SipB. Hence, we assessed the hemolytic activity of a Δ*iacP S*. Typhimurium strain complemented with various versions of *iacP* on sRBCs (Fig. 3). The strain producing the IacP variant D37A was affected similarly as that producing Δ*iacP*, showing that the D37 residue is crucial for the interaction of IacP with SipB. Only one third of the IacP-dependent hemolytic activity was restored when Δ*iacP* was complemented with the IacP variants L30A and L48A. Approximately two third of IacP-dependent hemolytic activity was restored when Δ*iacP* was complemented with the IacP variants L41T and L61A. Finally, the E32A substitution, which was shown to alter the IacP/SipB interaction by the two-

hybrid experiments, provided full hemolytic activity.

The results are summarized in Table 2. Overall, although the two-hybrid results showed more pronounced defects than those actually observed with the hemolysis assays, most of the point substitutions of IacP that affected the interaction with SipB (Fig. 3) also impaired hemolytic activity.

Conservation of the key residues of IacP involved in the IacP/SipB interaction- Next, we examined how the set of residues that we found to be involved in the interaction with SipB are conserved among acyl carrier proteins, either associated with SPI-1-like T3SS or fatty acid synthesis. Protein sequences of acyl carrier proteins genetically associated with SPI-1-like T3SS were retrieved [11], as well as those of acyl carrier proteins involved in fatty acid synthesis for the same bacterial species (Fig. 4).

Inspection of the multiple sequence alignment showed residues L30, V31, E32, D37, S38, L39, and L48 of IacP, necessary for its interaction with SipB according to the two-hybrid experiments, to be identical or similar among all examined acyl carrier proteins, whether they are associated with SPI-1-like T3SS or fatty acid synthesis. However, strikingly, the L41 and L61 residues of IacP, also required for unaltered complex formation, appeared to be conserved and specific to acyl carrier proteins associated with SPI-1-like T3SS only. A residue distinct in nature was found at the corresponding positions in the sequences of other acyl carrier proteins. Indeed, although a leucine residue was present at the L41 position of IacP in the sequences of acyl carrier proteins associated with SPI-1-like T3SS, a small polar residue, threonine, was at the same position in the sequences of acyl carrier proteins involved in fatty

acid synthesis (*S.* Typhimurium $IacP_{L41}$ *versus* ACP_{T39}) (Fig. 4). Similarly, the large hydrophobic residues (L, I, V, F or W) present at the L61 position of IacP in the sequences of acyl carrier proteins associated with SPI-1-like T3SS were substituted by a small hydrophobic residue, alanine, at the same position in the sequences of other acyl carrier proteins (*S.* Typhimurium $IacP_{L61}$ *versus* ACP_{A59}) (Fig. 4).

Interaction between proteins homologous to IacP and SipB from other bacteria- Because the residues L41 and L61 of IacP were specifically conserved in acyl carrier proteins associated with T3SS, we wished to evaluate their importance in the establishment of the interaction between orthologous proteins of IacP and SipB. However, we first had to demonstrate the existence of an interaction between homologous proteins. Indeed, the interaction between IacP and SipB and the subsequent acylation of the major hydrophobic translocator has only thus far been demonstrated in *Salmonella*. However, the genetic association of SPI-1-like T3SS and acyl carrier proteins has been observed in several - and -proteobacteria, suggesting a conserved functional association [11].

We therefore investigated the interaction between the acyl carrier protein and the major hydrophobic translocator associated with the SPI-1-like T3SS, encoded by the enteropathogen *Shigella flexneri* and the plant colonizer *Pseudomonas fluorescens,* using bacterial two-hybrid assays. We observed a positive interaction between IacP and IpaB from *S. flexneri* as well as between IacP and SipB from *P. fluorescens* (Fig. 5A-5C).

Then, we assessed whether replacement of the conserved serine by a threonine residue also abolished the interaction with the major hydrophobic translocator, as we previously

established that the catalytic serine, receiving the 4'-PP prosthetic group, is necessary for the interaction between IacP and SipB in *S.* Typhimurium (see S38T in Fig. 2 and [11]). This was indeed true, as variant S35T of *S. flexneri* IacP and S44T of *P. fluorescens* IacP no longer interacted with their respective major hydrophobic translocators (Fig. 5A).

Finally, we tested whether substitutions of the two residues that we found to be specifically conserved in acyl carrier proteins associated with SPI-1-like T3SS (L41 and L61 of *S.* Typhimurium IacP) affected the interaction with the major hydrophobic translocators of *S. flexneri* and *P. fluorescens*. Replacement of these residues in IacP from *S. flexneri* (variants L38T and L58A) and *P. fluorescens* (variants L47T and V67A) indeed altered the interaction with their respective T3SS-translocators (Fig. 5A). A western blot with an antibody directed against the T18 domain showed that the T18-IacP mutants of *S. flexneri* were produced (Fig. S1B).

The leucine residues conserved among acyl carrier proteins associated with SPI-1 T3SS are necessary but not sufficient to their promote interaction with the major hydrophobic translocator- The analysis of multiple sequence alignments showed L41 and L61 of IacP to be specifically conserved in acyl carrier proteins associated with SPI-1-like T3SS. Furthermore, the bacterial two-hybrid experiments performed with proteins derived from *S.* Typhimurium, *S. flexneri*, and *P. fluorescens* showed the involvement of these residues in their interaction with the major hydrophobic translocator. We therefore introduced these residues at the corresponding positions in *S.* Typhimurium ACP, which is not able to interact with SipB, to test whether their presence was sufficient to promote an interaction with SipB. The T39 and A59 residues of ACP were substituted for a leucine residue. However, such

substitutions were not sufficient to promote an interaction between ACP and SipB (see ACP_{T39L} and $ACP_{T39L\ A59L}$ Fig. 5B). Moreover, the sole replacement of T39 by a leucine residue in ACP was not compatible with the essential functions of this protein. Indeed, the temperature-sensitive *E. coli* ACP^{ts} strain could not be complemented with ACP_{T39L}, whereas it was with the wildtype version (Fig. S2). In conclusion, the characteristic residues of acyl carrier proteins associated with SPI-1-like T3SS are not compatible with the essential functions of ACP, and this might explain the necessity to acquire a specific acyl carrier protein dedicated to the major T3SS hydrophobic translocator.

We also tested whether another acyl carrier protein naturally harboring leucine residues at positions L41 and/or L61 of IacP could interact with SipB from *S.* Typhimurium. We thus used the acyl carrier proteins associated with the SPI-1-like T3SS of *S. flexneri* and *P. fluorescens*. However, no interactions were detected, suggesting that the acyl carrier protein associated with a SPI-1-like T3SS in one species is highly specific and cannot function in another (Fig. 5C). This shows that there must be further specificity determinants to explain the species-specific interaction between the acyl carrier protein and the major hydrophobic translocator.

DISCUSSION

We investigated the residues located at the interface of the IacP/SipB complex to understand which determinants of IacP drive its specific interaction with SipB using a combined approach of structural biology and biological assays. Based on NMR chemical shift mapping, we substituted 17 of 82 residues of IacP to test their contribution to its interaction with SipB. Nine (L30, V31, E32, D37, S38, L39, L41, L48, and L61) were necessary to establish the interaction with SipB, as shown by the bacterial two-hybrid method (Table 2). We generated a 3D structural model of IacP, using the Phyre2 Protein fold recognition server, to visualize where these residues are located in the IacP structure. Most of the residues necessary for the interaction with SipB covered the surface of IacP around the 4'-PP binding site (Fig. 6A). As discussed below, the prosthetic group appears to be involved in the interaction. Seven of these nine residues were conserved in all acyl carrier proteins that we examined in this study and two (L41 and L61) appeared to be specific to acyl carrier proteins associated with SPI-1-like T3SS. As suggested below, these two residues may promote solvent exposition of acyl-4'-PP to mediate the interaction with SipB. Finally, among the 17 residues highlighted by the NMR approach, point substitution of eight did not affect the interaction between IacP and SipB, as shown by the bacterial two-hybrid method. These residues are adjacent to those described in the 3D structural model of IacP (Fig. 6B), they might have been pointed by the NMR approach because of collateral effects from neighboring residues. Alternatively, because these residues are not conserved among acyl carrier proteins (Fig. 4), they might be important for the specificity of the interaction between the two partners rather than its stabilization.

Contribution of 4'-PP to the specific interaction between IacP and SipB- We show that acyl carrier proteins associated with SPI-1-like T3SS do not interact with the corresponding major hydrophobic translocator in the absence of 4'-PP. Indeed, the variants S38T and L39A of *S.* Typhimurium IacP that were devoid of 4'-PP did not interact with SipB (Tables 1 and 2) and prevention of 4'-PP addition by substitution of the conserved serine of *S. flexneri* and *P. fluorescens* IacP also abrogated the interaction with $IpaB_{sfl}$ and $SipB_{pfe}$, respectively (Fig. 5A). We therefore suggest that 4'-PP itself participates in the interaction and has to be appropriately exposed. This may be the contribution of the residues L41 and L61 of IacP, which are specifically conserved in acyl carrier proteins associated with SPI-1-like T3SS. These residues are located at the entrance of the hydrophobic pocket (Fig. 6C) and may control which chemical groups enter the cavity. Indeed, acyl carrier proteins found in *Streptomyces coelicolor*, involved either in polyketide or fatty acid synthesis, display moderately bulky hydrophobic residues (L, M and V) at one or both positions corresponding to L41 and L61 of IacP. Interestingly, the thioester bound of the acyl-4'-PP in these acyl carrier proteins is not sequestered in the hydrophobic pocket but rather exposed to the solvent (Fig. 6D) [27–29]. In contrast, acyl carrier proteins involved in fatty acid synthesis in *E. coli* and the bacterial species that we analyzed in this study, display a threonine (T39) and alanine (A59) at the positions corresponding to L41 and L61 of IacP (Fig. 4). These residues play a key role in the stabilization of 4'-PP in a binding mode, in which the acylated prosthetic group is inserted in the hydrophobic cavity of the protein (Fig. 6E) [30]. This structural information suggests that L41 and L61 allow adequate protuberance of 4'-PP at the entrance of the hydrophobic cavity, leading to the proper conformation to interact with SipB. Substitution of one of these residues only weakens the interaction between the two partners, as demonstrated by the hemolysis test, which assesses the functionality of the IacP/SipB interaction in

S. Typhimurium (Fig. 3). In contrast, the bacterial two-hybrid method showed the complete absence of interaction with each of the point variants. This is not surprising, as we previously observed that this method fails to detect residual interactions below a certain threshold [31]. This property provides an advantage because it still indicates amino acids that contribute to an interaction without the need for multiple substitutions to completely break it. Indeed, multiple substitutions may increase the chance to compromise 3D folding of the protein. For example, the residue E32, whose substitution did not impair the interaction between IacP and SipB as reported by the hemolysis assay (Fig. 3), was revealed by the bacterial two-hybrid method, even if this substitution was the less impacting the interaction also by this method (Fig. 2).

Other contributions to the specific interaction between IacP and SipB- Studies of ACP in *E. coli* have shown that both the prosthetic group and acyl chain contact the surface of the partner enzyme [32, 33]. Hence, in addition to the involvement of 4'-PP, the acyl chain itself may participate in the establishment of the interaction between IacP and SipB. However, this was difficult to determine, as the purified IacP with which the *in vitro* experiments were performed was clearly bound to 4'-PP but did not show evidence of acylation.

The anionic -helix 2 of ACP involved in fatty acid synthesis is called the "recognition" helix, because it mediates interactions with many partner enzymes [12, 13]. However, we did not identify anionic residues of -helix 2 of IacP that were involved in the interaction with SipB. Indeed, these residues are not well conserved among acyl carrier proteins associated with SPI-1-like T3SS (Fig. 4). Instead, we found residues E32 and, especially, D37 of loop 1-2 to be crucial for the interaction with SipB. The substitution of D37 affected the interaction as strongly as the absence of 4'-PP, both in the two-hybrid and hemolytic tests. Although this

residue belongs to the 4'-PP binding motif and establishes the hydrophilic interaction between ACP and its holo-ACP synthase in *Bacillus subtilis* [34], our results indicate that the IacP variant D37A carries the prosthetic group. We therefore suggest that D37 establishes a key salt bridge to lock the interaction with SipB.

Finally, this study also showed that the interaction between IacP and SipB is conserved, using the homologous proteins from *S. flexneri* and *P. fluorescens* (Fig. 5A). However, the protein pairs were not interchangeable (Fig. 5C). Interestingly, there is great variability among the sequences of both acyl carrier proteins (14 to 45% identity between genera) (Fig. 4) and major hydrophobic translocators (16 to 63% identity between genera) associated with SPI-1-like T3SS. This is in contrast with the high conservation observed among acyl carrier proteins involved in fatty acid synthesis (72 to 100% identity between genera) (Fig. 4). Such sequence variability is consistent with the fact that the translocon constitutes an extracellular part of the T3SS machinery prone to rapid evolution to adapt to the host eukaryotic cell and its ecological niche [35]. The variability in sequences mirrored at the level of the genetically associated acyl carrier protein suggests specific adaptation between the two partners within bacterial species. The residues that we identified to affect the interaction are similar or identical to those in other acyl carrier proteins associated with SPI-1-like T3SS. Thus, these residues may not explain the high specificity of recognition between acyl carrier protein/ translocator pairs. However, residues N25, G26, F46, G47, S49, C56, and F67 of IacP were affected by complex formation in the NMR experiment but point mutations did not affect the IacP/SipB interaction (Fig. 2). These are among the variable residues in acyl carrier proteins associated with SPI-1-like T3SS and hence they may play a role in the specific recognition of the translocator. However, we could not establish that they are driving forces in complex formation.

ACKNOWLEDGEMENTS

We thank Pamela Schnupf, from the Sansonetti lab at that time (Pasteur Institut, Paris, France) and Marta Martín Basanta (Universidad Autónoma de Madrid, Spain), for their kind gifts of genomic DNA from *S. flexneri* and *P. fluorescens*, respectively. We thank Allison Huguenot for the generation of pEB1439. We thank Tâm Mignot for critical reading of the manuscript and all members of LISM for fruitful discussions. We thank A. Edelman and associates for correcting this manuscript. This work was funded by the Aix-Marseille Université (AMU) and the Centre National de la Recherche Scientifique (CNRS). MJC was a recipient of a doctoral fellowship from the French Ministère de l'Enseignement Supérieur et de la Recherche.

CONFLICT OF INTERESTS STATEMENT

The authors declare no conflict of interests with the contents of this article.

REFERENCES

[1] LaRock, D.L., Chaudhary, A. and Miller, S.I. (2015) *Salmonellae* interactions with host processes. *Nat Rev Microbiol* **13**, 191-205.

[2] Mattei, P.J., Faudry, E., Job, V., Izore, T., Attree, I. and Dessen, A. (2011) Membrane targeting and pore formation by the type III secretion system translocon. *FEBS J* **278**, 414-426.

[3] Diepold, A. and Armitage, J.P. (2015) Type III secretion systems: the bacterial flagellum and the injectisome. *Philos Trans R Soc Lond B Biol Sci* **370**,

[4] Notti, R.Q. and Stebbins, C.E. (2016) The Structure and Function of Type III Secretion Systems. *Microbiol Spectr* **4**,

[5] Myeni, S.K., Wang, L. and Zhou, D. (2013) SipB-SipC complex is essential for translocon formation. *PLoS One* **8**, e60499.

[6] Barta, M.L., Dickenson, N.E., Patil, M., Keightley, A., Wyckoff, G.J., Picking, W.D., Picking, W.L. and Geisbrecht, B.V. (2012) The structures of coiled-coil domains from type III secretion system translocators reveal homology to pore-forming toxins. *J Mol Biol* **417**, 395-405.

[7] Tucker, S.C. and Galán, J.E. (2000) Complex function for SicA, a *Salmonella enterica* serovar Typhimurium type III secretion-associated chaperone. *J Bacteriol* **182**, 2262-2268.

[8] Kim, B.H., Kim, H.G., Kim, J.S., Jang, J.I. and Park, Y.K. (2007) Analysis of functional domains present in the N-terminus of the SipB protein. *Microbiology* **153**, 2998-3008.

[9] Lunelli, M., Lokareddy, R.K., Zychlinsky, A. and Kolbe, M. (2009) IpaB-IpgC interaction defines binding motif for type III secretion translocator. *Proc Natl Acad Sci U S A* **106**, 9661-9666.

[10] Discola, K.F., Forster, A., Boulay, F., Simorre, J.P., Attree, I., Dessen, A. and Job, V. (2014) Membrane and chaperone recognition by the major translocator protein PopB of the type III secretion system of *Pseudomonas aeruginosa*. *J Biol Chem* **289**, 3591-3601.

[11] Viala, J.P., Prima, V., Puppo, R., Agrebi, R., Canestrari, M.J., Lignon, S., Chauvin, N., Méresse, S., Mignot, T., Lebrun, R. and Bouveret, E. (2017) Acylation of the Type 3 Secretion System Translocon Using a Dedicated Acyl Carrier Protein. *PLoS Genet* **13**, e1006556.

[12] Byers, D.M. and Gong, H. (2007) Acyl carrier protein: structure-function relationships in a conserved multifunctional protein family. *Biochem Cell Biol* **85**, 649-662.

[13] Chan, D.I. and Vogel, H.J. (2010) Current understanding of fatty acid biosynthesis and the acyl carrier protein. *Biochem J* **430**, 1-19.

[14] El-Gebali, S., Mistry, J., Bateman, A., Eddy, S.R., Luciani, A., Potter, S.C., Qureshi, M., Richardson, L.J., Salazar, G.A., Smart, A., Sonnhammer, E.L.L., Hirsh, L., Paladin, L., Piovesan, D., Tosatto, S.C.E. and Finn, R.D. (2018) The Pfam protein families database in 2019. *Nucleic Acids Res*

[15] Cronan, J.E. (2018) Advances in synthesis of biotin and assembly of lipoic acid. *Curr Opin Chem Biol* **47**, 60-66.

[16] Linhartová, I., Bumba, L., Mašín, J., Basler, M., Osička, R., Kamanová, J., Procházková, K., Adkins, I., Hejnová-Holubová, J., Sadílková, L., Morová, J. and Sebo, P. (2010) RTX proteins: a highly diverse family secreted by a common mechanism. *FEMS Microbiol Rev* **34**, 1076-1112.

[17] Butland, G., Peregrin-Alvarez, J.M., Li, J., Yang, W., Yang, X., Canadien, V., Starostine, A., Richards, D., Beattie, B, Krogan, N., Davey, M., Parkinson, J., Greenblatt, J. and Emili, A. (2005) Interaction network containing conserved and essential protein complexes in *Escherichia coli*. *Nature* **433**, 531-537.

[18] Gully, D., Moinier, D., Loiseau, L. and Bouveret, E. (2003) New partners of acyl carrier protein detected in *Escherichia coli* by tandem affinity purification. *FEBS Lett* **548**, 90-96.

[19] Karimova, G., Pidoux, J., Ullmann, A. and Ladant, D. (1998) A bacterial two-hybrid system based on a reconstituted signal transduction pathway. *Proc Natl Acad Sci U S A* **95**, 5752-5756.

[20] Gully, D. and Bouveret, E. (2006) A protein network for phospholipid synthesis uncovered by a variant of the tandem affinity purification method in *Escherichia coli*. *Proteomics* **6**, 282-293.

[21] Miller, J.H. (1992) A short course in bacterial genetics: a laboratory manual and handbook for *Escherichia coli* and related bacteria., Cold Spring Harbor, NY: Cold Spring Harbor Laboratory Press.

[22] Wahl, A., My, L., Dumoulin, R., Sturgis, J.N. and Bouveret, E. (2011) Antagonistic regulation of *dgkA* and *plsB* genes of phospholipid synthesis by multiple stress responses in *Escherichia coli*. *Mol Microbiol* **80**, 1260-1275.

[23] Vourtsis, D.J., Chasapis, C.T., Pairas, G., Bentrop, D. and Spyroulias, G.A. (2014) NMR conformational properties of an Anthrax Lethal Factor domain studied by multiple amino acid-selective labeling. *Biochem Biophys Res Commun* **450**, 335-340.

[24] Viala, J.P., Puppo, R., My, L. and Bouveret, E. (2013) Posttranslational maturation of the invasion acyl carrier protein of *Salmonella enterica* serovar Typhimurium requires an essential phosphopantetheinyl transferase of the fatty acid biosynthesis pathway. *J Bacteriol* **195**, 4399-4405.

[25] Keller, R. (2004) Computer aided resonance assignment tutorial.

[26] Battesti, A. and Bouveret, E. (2012) The bacterial two-hybrid system based on adenylate cyclase reconstitution in *Escherichia coli*. *Methods* **58**, 325-334.

[27] Evans, S.E., Williams, C., Arthur, C.J., Płoskoń, E., Wattana-amorn, P., Cox, R.J., Crosby, J., Willis, C.L., Simpson, T.J. and Crump, M.P. (2009) Probing the Interactions of early polyketide intermediates with the Actinorhodin ACP from *S. coelicolor* A3(2). *J Mol Biol* **389**, 511-528.

[28] Płoskoń, E., Arthur, C.J., Kanari, A.L., Wattana-amorn, P., Williams, C., Crosby, J., Simpson, T.J., Willis, C.L. and Crump, M.P. (2010) Recognition of intermediate functionality by acyl carrier protein over a complete cycle of fatty acid biosynthesis. *Chem Biol* **17**, 776-785.

[29] Crosby, J. and Crump, M.P. (2012) The structural role of the carrier protein--active controller or passive carrier. *Nat Prod Rep* **29**, 1111-1137.

[30] Roujeinikova, A., Simon, W.J., Gilroy, J., Rice, D.W., Rafferty, J.B. and Slabas, A.R. (2007) Structural studies of fatty acyl-(acyl carrier protein) thioesters reveal a hydrophobic binding cavity that can expand to fit longer substrates. *J Mol Biol* **365**, 135-145.

[31] Angelini, S., My, L. and Bouveret, E. (2012) Disrupting the Acyl Carrier Protein/SpoT interaction in vivo: identification of ACP residues involved in the interaction and consequence on growth. *PLoS One* **7**, e36111.

[32] Nguyen, C., Haushalter, R.W., Lee, D.J., Markwick, P.R., Bruegger, J., Caldara-Festin, G., Finzel, K., Jackson, D.R., Ishikawa, F., O'Dowd, B., McCammon, J.A., Opella, S.J., Tsai, S.C. and Burkart, M.D. (2014) Trapping the dynamic acyl carrier protein in fatty acid biosynthesis. *Nature* **505**, 427-431.

[33] Masoudi, A., Raetz, C.R., Zhou, P. and Pemble, C.W. (2014) Chasing acyl carrier protein through a catalytic cycle of lipid A production. *Nature* **505**, 422-426.

[34] Parris, K.D., Lin, L., Tam, A., Mathew, R., Hixon, J., Stahl, M., Fritz, C.C., Seehra, J. and Somers, W.S. (2000) Crystal structures of substrate binding to *Bacillus subtilis* holo-(acyl

carrier protein) synthase reveal a novel trimeric arrangement of molecules resulting in three active sites. *Structure* **8**, 883-895.

[35] Abby, S.S. and Rocha, E.P. (2012) The non-flagellar type III secretion system evolved from the bacterial flagellum and diversified into host-cell adapted systems. *PLoS Genet* **8**, e1002983.

[36] Battesti, A. and Bouveret, E. (2009) Bacteria possessing two RelA/SpoT-like proteins have evolved a specific stringent response involving the acyl carrier protein-SpoT interaction. *J Bacteriol* **191**, 616-624.

[37] Waterhouse, A.M., Procter, J.B., Martin, D.M., Clamp, M. and Barton, G.J. (2009) Jalview Version 2--a multiple sequence alignment editor and analysis workbench. *Bioinformatics* **25**, 1189-1191.

[38] Qiu, X. and Janson, C.A. (2004) Structure of apo acyl carrier protein and a proposal to engineer protein crystallization through metal ions. *Acta Crystallogr D Biol Crystallogr* **60**, 1545-1554.

[39] Kelley, L.A., Mezulis, S., Yates, C.M., Wass, M.N. and Sternberg, M.J. (2015) The Phyre2 web portal for protein modeling, prediction and analysis. *Nat Protoc* **10**, 845-858.

[40] Keating, D.H., Carey, M.R. and Cronan, J.E.J. (1995) The unmodified (apo) form of *Escherichia coli* acyl carrier protein is a potent inhibitor of cell growth. *J Biol Chem* **270**, 22229-22235.

[41] Keating, D.H. and Cronan, J.E. (1996) An isoleucine to valine substitution in *Escherichia coli* acyl carrier protein results in a functional protein of decreased molecular radius at elevated pH. *J Biol Chem* **271**, 15905-15910.

Table 1. **Maturation status of IacP mutants impaired in their interaction with SipB**

The masses of purified intact wildtype and mutant versions of $_{6His-}$IacP were determined by MALDI-TOF mass spectrometry and are given in Daltons. Theoretical masses are indicated for a protein devoid of the start methionine. The theoretical mass closest to the experimental mass is shown in bold.

$_{6His-}$IacP Mutant	**Theoretical mass w/out 4'-PP**	**Theoretical mass w/ 4'-PP**	**Experimental mass observed**
Wildtype	11768	**12107**	12104
L30A	11726	**12065**	12059
V31A	11740	**12079**	12074
E32A	11710	**12049**	12043
D37A	11724	**12063**	12056
S38T	**11782**	12121	11781
L39A	**11726**	12065	11721
L41T	11756	**12095**	12092
L48A	11726	**12065**	12059
L61A	11726	**12065**	12060

Table 2. **Summary of the analysis made on IacP variants**

Summary of the data presented in Figures 2, 3 and Table 1. The first column indicates the substitution made in IacP. The second column indicates whether an interaction was detected (+) or not (-) between IacP and SipB by the bacterial two-hybrid assay. The third column indicates whether the IacP variant was modified by the addition of 4'-PP, as indicated by mass spectrometry. In the last column, S. Typhimurium SL1344 Δ*iacP* was complemented with the indicated version of IacP and hemolytic activity on sRBC ranked between the negative (- for no IacP) and positive controls (+++ for wildtype IacP).

IacP :	**2H IacP/SipB**	**4'-PP**	**Hemolysis**
No IacP	/	/	-
WT	+	+	+++
L30A	-	+	+
V31A	-	+	++
E32A	-	+	+++
D37A	-	+	-
S38T	-	-	-
L39A	-	-	NT
L41T	-	+	++
L48A	-	+	+
L61A	-	+	++

Table 3. **Bacterial strains used in this study**

Name	Lab n°	Description and Resistance	Reference
Escherichia coli			
DH5α	EB070	*fhuA*2 Δ(*argF-lacZ*)U169 *phoA gln*V44 Φ80 Δ(*lacZ*)M15 *gyrA*96 *recA*1 *relA*1 *endA*1 *thi*-1 *hsdR*17	Lab stock
BTH101	EB003	F-, *cya*-99, *araD*139, *galE*15, *galK*16, *rpsL*1 (Str r), *hsdR*2, *mcrA*1, *mcrB*1.	[19]
BL21 (DE3) pLys	EB072	F- *ompT gal dcm lon hsdSB* (rB- mB-) λ(DE3) pLysS(cmR)	Lab stock
MG1655	EB944	F^- λ^- ilvG- rfb-50 rph-1	Lab stock
ACP^{ts}	EB337	MG1655 $acpP_{D38V}{}^{ts}$ Δ*fabF*::Cm^R	[36]
***Salmonella enterica* serovar Typhimurium SL1344**			
WT	JV112		Lab stock
Δ*iacP*	JV113	Δ*iacP*:: kan^R	[11]
Δ*sipB*	JV114	Δ*sipB*:: kan^R	[11]

FIGURE LEGENDS

Figure 1. **^{1}H-^{15}N HSQC spectra of *S.* Typhimurium IacP**

A) The sequence assignment of IacP is indicated by amino-acid numbering. A zoom of the center of the spectrum is also shown to simplify the figure. **B)** Purified proteins used to map the IacP residues affected by the interaction with SipB. ^{15}N-labeled IacP is shown in the left lane and the SipB/SicA complex in the right. Numbers indicate the molecular weight in kDa. **C)** Zoom of the ^{1}H-^{15}N HSQC spectrum of ^{15}N-labeled IacP incubated with one equivalent of the SipB/SicA complex (in red) superimposed over the ^{1}H-^{15}N HSQC of ^{15}N-labeled IacP (in blue). **D)** Zoom of the ^{1}H-^{15}N HSQC spectrum of ^{15}N-labeled IacP incubated with one equivalent of SicA (in red) superimposed over the ^{1}H-^{15}N HSQC spectrum of ^{15}N-labeled IacP (in blue).

Figure 2. **Residues of IacP necessary for the interaction with SipB as measured by the bacterial two-hybrid assay**

Interactions between pairs of hybrid proteins, resulting from the fusion of the indicated protein with the T18 and T25 fragments of *B. pertussis* adenylate cyclase, were assayed by measuring β-galactosidase activity using the bacterial two-hybrid method in *E. coli* BTH101. A dash indicates the absence of translational fusion with the T18 or T25 fragment. The chaperone SicA was co-produced with the various T18_IacP hybrids from an artificial operon

constructed on the two-hybrid vector. The values represent the mean of three biological independent assays. Error bars indicate the standard deviation.

Figure 3. **Hemolytic activity of *S.* Typhimurium on sheep Red Blood Cells**

The hemolytic activity of Δ*iacP* (delimited by the dashed line), producing various point mutants of IacP from pP_{TET}, was compared to that of wildtype *S.* Typhimurium SL1344 on sRBC. The part of the hemolytic activity due to a functional interaction between IacP and SipB (leading to SipB acylation) is shown above the dashed line. The hemolytic activity of Δ*sipB* is shown as a negative control. Hemolytic activity was followed by measuring hemoglobin release at 542 nm and normalized to the hemolytic activity of WT pP_{TET}, which was set to 100%. The hemolysis was assayed in triplicate and the error bars represent error propagation. Unpaired t-tests were applied. The stars indicate values that were statistically significantly different from those of WT pP_{TET}. ***$p < 0.0005$, **$p < 0.005$, *$p < 0.05$

Figure 4. **Multiple sequence alignment of acyl carrier proteins associated with SPI-1-like T3SS or fatty acid synthesis**

Circles indicate the residues of IacP that were identified by the NMR approach to have a different environment when IacP was incubated with the SipB/SicA complex. Empty circles: substitution of the corresponding residue does not affect the interaction with SipB (Fig. 2). Filled circles: substitution of the corresponding residue affects the interaction with SipB as measured by the bacterial two-hybrid assay (Fig. 2). Grey circles: not tested. The star indicates the conserved serine residue to which 4'-PP is attached. Arrowheads indicate the

residues L41 and L61 of IacP, which are conserved in acyl carrier proteins associated with SPI-1-like T3SS, but not those associated with fatty acid synthesis. Residues that are boxed correspond to the 4'-PP-binding motif. Dashes underline α-helices ascribed to ACP [13]. The multiple sequence alignment was created using Clustal omega and was edited with Jalview [37]. Bacterial species from which protein sequences were retrieved were *Salmonella* Typhimurium LT2 (stm), *Salmonella bongori* NCTC 12419 (sbg), *Chromobacterium violaceum* ATCC 12472 (cvi), *Shigella flexneri* M90T (sflM90T), *Shigella dysenteriae* Sd197 (sdy), *Shigella sonnei* Ss046 (ssn), *Pseudomonas fluorescens* F113 (pfeF113), *Pseudomonas sp*. UW4 (ppuu), *Providencia stuartii* MRSN 2154 (psiMRSN2154), *Yersinia enterocolitica subsp. enterocolitica* 8081 (yen8081), *Burkholderia thailandensis* MSMB121 (btd), *Burkholderia pseudomallei* 668 (bpd), *Burkholderia mallei* NCTC 10247 (bmn), *Erwinia amylovora* ATCC 49946 (eay), and *Erwinia tasmaniensis* Et1/99 (eta).

Figure 5. **Interactions between acyl carrier proteins and major hydrophobic translocators associated with SPI-1-like T3SS assayed by the bacterial two-hybrid assays**.

Interactions between pairs of hybrid proteins, resulting from the fusion of the indicated protein with the T18 and T25 fragments of *B. pertussis* adenylated cyclase, were assayed using the bacterial two-hybrid method in *E. coli* BTH101. A positive interaction is indicated by β-galactosidase activity (measured in triplicate, error bars represent the standard error) (A-B) or blue staining on LB agar medium supplemented with IPTG and X-Gal (C). The three-letter code indicates from which organism the genes were cloned: stm for *S*. Typhimurium 12023, sfl for *S. flexneri* M90T, and pfe for *P. fluorescens* F113. A dash

indicates the absence of translational fusion with the T18- or T25- fragment. We previously observed that the co-production of the chaperone SicA was necessary to visualize the interaction between IacP and SipB [11]. Therefore, an artificial operon was created on the two-hybrid vector to co-express the hybrid T25- or T18-major hydrophobic translocator with its chaperone (SicA for *S*. Typhimurium, IpgD for *S. flexneri*, and YopD for *P. fluorescens*).

Figure 6. **Location of amino-acid residues of IacP that are involved in the interaction with SipB in a 3D structural model**

A-B) The structure of IacP was modeled from *E. coli* ACP, which is involved in fatty acid synthesis (PDB : 1t8k) [38], with which IacP shares 30% identity. The structure of IacP was modeled with a 99.7% confidence score using the intensive modeling mode of the Phyre2 website [39]. Residues that were found to be important for the interaction with SipB by the bacterial two-hybrid method are shown in yellow and the conserved serine residue, which binds 4'-PP, is shown in red (A-B). Residues that were designated to be at the interface of the IacP/SipB complex by the NMR approach, but not found to be necessary for the interaction by the bacterial two-hybrid method, are shown in pale brown (B). Cartoon representation and sphere representation, front and back (rotated 180°, y axis) are shown in the left and right panels, respectively. **C)** Sphere representation of the 3D structural model of IacP. Residues L41 and L61, shown in yellow, are located at the entrance of the hydrophobic cavity. The conserved serine is shown in red. **D-E**) Sphere representation of the 3D structures of the hexanoyl-acyl carrier proteins (blue) involved in the synthesis of the polyketide actinorhodin ($actACP_{sco}$) in *S. coelicolor* (PDB: 2KGA) [27] (D) or fatty acid synthesis in *E. coli* (ACP_{eco}) (PDB: 2FAC) [30] (E). The conserved serine is shown in red. Residues found at the

corresponding positions of L41 and L61 in IacP are shown in pale green. The hexanoyl-4'-PP, shown as sticks, is exposed to solvent in actACP_{sco}, whereas it is inserted and hidden in the hydrophobic cavity of ACP_{eco}. The thioester bond (yellow), between the extremity of 4'-PP and the metabolite, is indicated by a white arrowhead in D because it is exposed to solvent and visible, but not in E because it is buried.

Figure 1

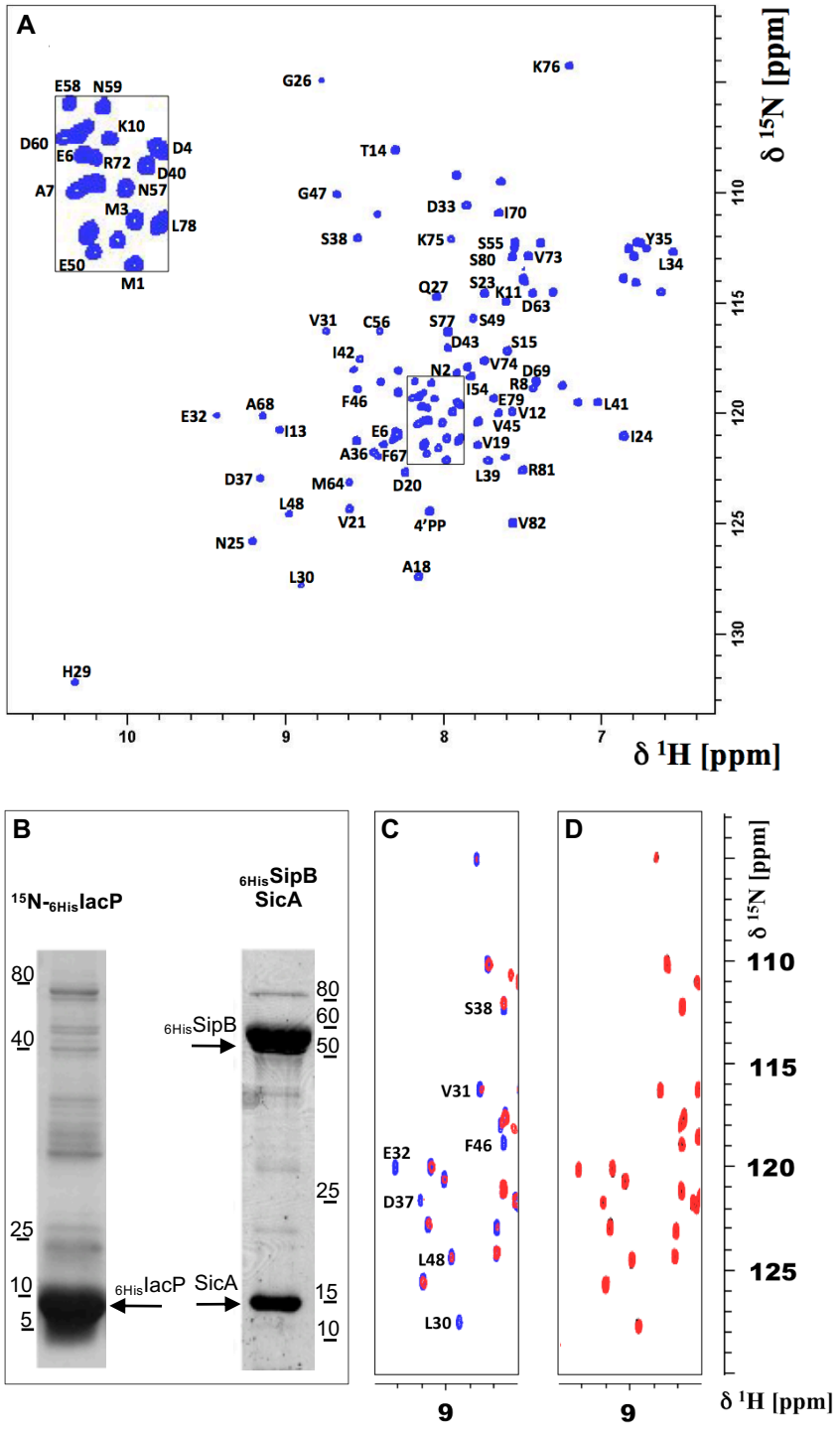


Figure 1. **^{1}H-^{15}N HSQC spectra of *S.* Typhimurium IacP**
A) The sequence assignment of IacP is indicated by amino-acid numbering. A zoom of the center of the spectrum is also shown to simplify the figure. **B)** Purified proteins used to map the IacP residues affected by the interaction with SipB. ^{15}N-labeled IacP is shown in the left lane and the SipB/SicA complex in the right. Numbers indicate the molecular weight in kDa. **C)** Zoom of the ^{1}H-^{15}N HSQC spectrum of ^{15}N-labeled IacP incubated with one equivalent of the SipB/SicA complex (in red) superimposed over the ^{1}H-^{15}N HSQC of ^{15}N-labeled IacP (in blue). **D)** Zoom of the ^{1}H-^{15}N HSQC spectrum of ^{15}N-labeled IacP incubated with one equivalent of SicA (in red) superimposed over the ^{1}H-^{15}N HSQC spectrum of ^{15}N-labeled IacP (in blue).

Figure 2

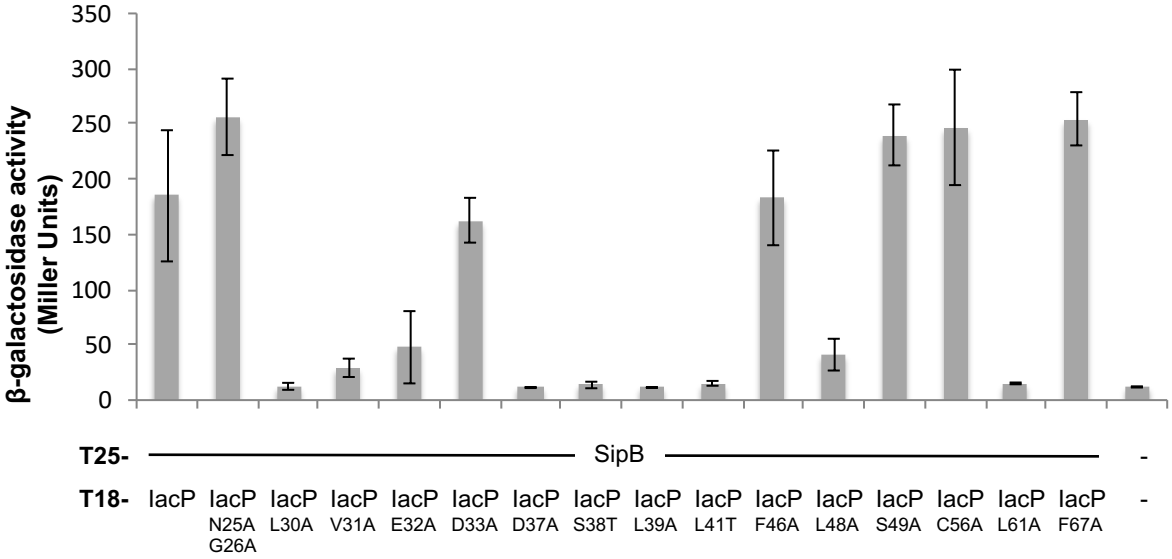


Figure 2. **Residues of IacP necessary for the interaction with SipB as measured by the bacterial two-hybrid assay**

Interactions between pairs of hybrid proteins, resulting from the fusion of the indicated protein with the T18 and T25 fragments of *B. pertussis* adenylate cyclase, were assayed by measuring β-galactosidase activity using the bacterial two-hybrid method in *E. coli* BTH101. A dash indicates the absence of translational fusion with the T18 or T25 fragment. The chaperone SicA was co-produced with the various T18_IacP hybrids from an artificial operon constructed on the two-hybrid vector. The values represent the mean of three biological independent assays. Error bars indicate the standard deviation.

Figure 3

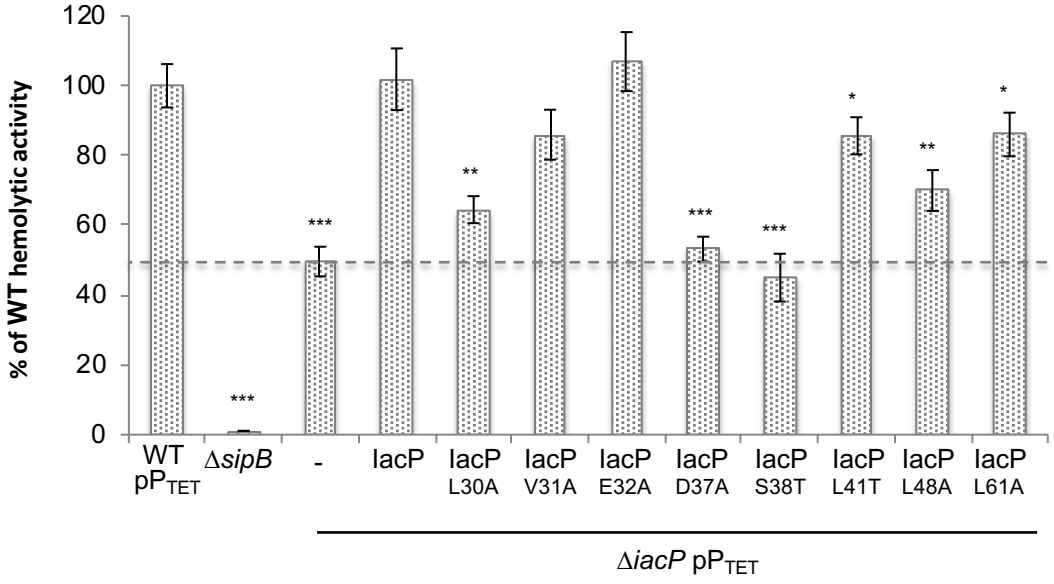


Figure 3. **Hemolytic activity of *S.* Typhimurium on sheep Red Blood Cells**
The hemolytic activity of Δ*iacP* (delimited by the dashed line), producing various point mutants of IacP from pP$_{TET}$, was compared to that of wildtype *S.* Typhimurium SL1344 on sRBC. The part of the hemolytic activity due to a functional interaction between IacP and SipB (leading to SipB acylation) is shown above the dashed line. The hemolytic activity of Δ*sipB* is shown as a negative control. Hemolytic activity was followed by measuring hemoglobin release at 542 nm and normalized to the hemolytic activity of WT pP$_{TET}$, which was set to 100%. The hemolysis was assayed in triplicate and the error bars represent error propagation. Unpaired t-tests were applied. The stars indicate values that were statistically significantly different from those of WT pP$_{TET}$. ***p < 0.0005, **p < 0.005, *p < 0.05

Figure 4

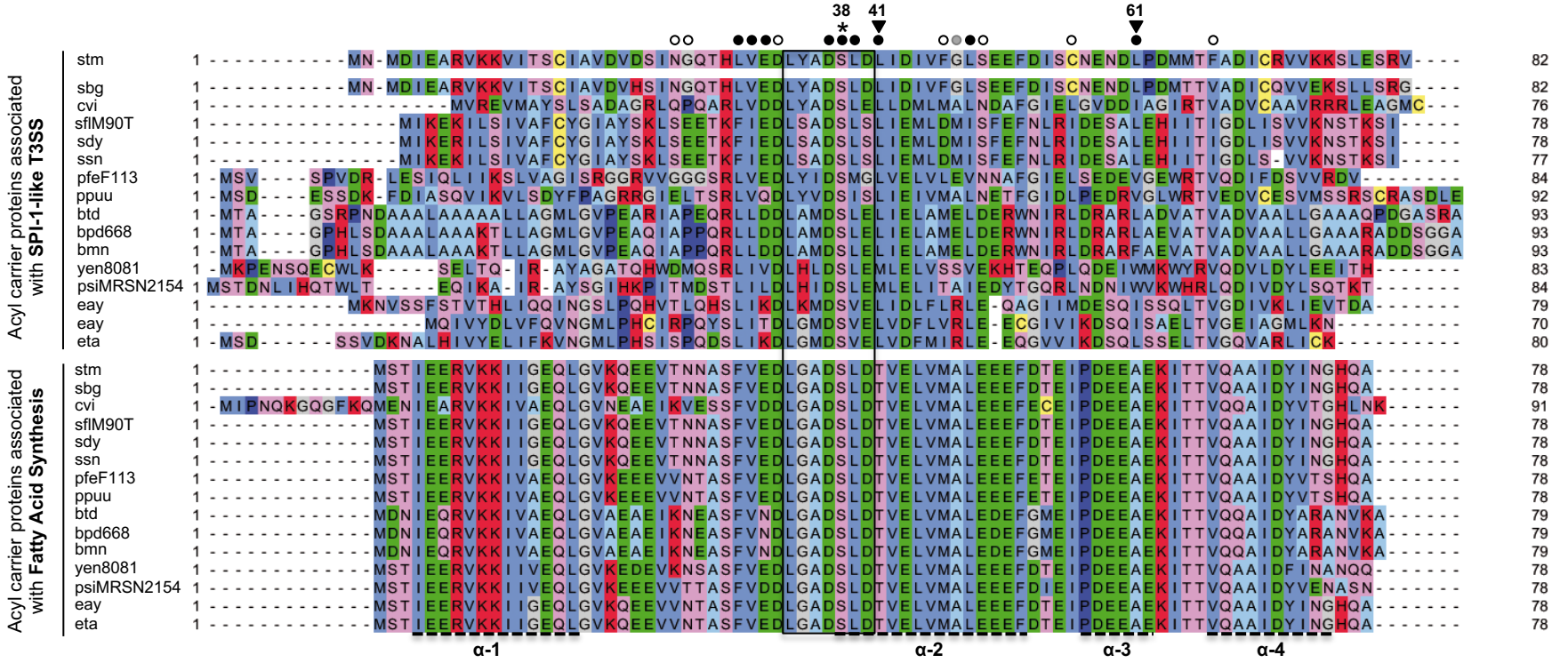


Figure 4. **Multiple sequence alignment of acyl carrier proteins associated with SPI-1-like T3SS or fatty acid synthesis**
Circles indicate the residues of IacP that were identified by the NMR approach to have a different environment when IacP was incubated with the SipB/SicA complex. Empty circles: substitution of the corresponding residue does not affect the interaction with SipB (Fig. 2). Filled circles: substitution of the corresponding residue affects the interaction with SipB as measured by the bacterial two-hybrid assay (Fig. 2). Grey circles: not tested. The star indicates the conserved serine residue to which 4'-PP is attached. Arrowheads indicate the residues L41 and L61 of IacP, which are conserved in acyl carrier proteins associated with SPI-1-like T3SS, but not those associated with fatty acid synthesis. Residues that are boxed correspond to the 4'-PP-binding motif. Dashes underline α-helices ascribed to ACP [13]. The multiple sequence alignment was created using Clustal omega and was edited with Jalview [37]. Bacterial species from which protein sequences were retrieved were *Salmonella* Typhimurium LT2 (stm), *Salmonella bongori* NCTC 12419 (sbg), *Chromobacterium violaceum* ATCC 12472 (cvi), *Shigella flexneri* M90T (sflM90T), *Shigella dysenteriae* Sd197 (sdy), *Shigella sonnei* Ss046 (ssn), *Pseudomonas fluorescens* F113 (pfeF113), *Pseudomonas sp*. UW4 (ppuu), *Providencia stuartii* MRSN 2154 (psiMRSN2154), *Yersinia enterocolitica subsp. enterocolitica* 8081 (yen8081), *Burkholderia thailandensis* MSMB121 (btd), *Burkholderia pseudomallei* 668 (bpd), *Burkholderia mallei* NCTC 10247 (bmn), *Erwinia amylovora* ATCC 49946 (eay), and *Erwinia tasmaniensis* Et1/99 (eta).

Figure 5

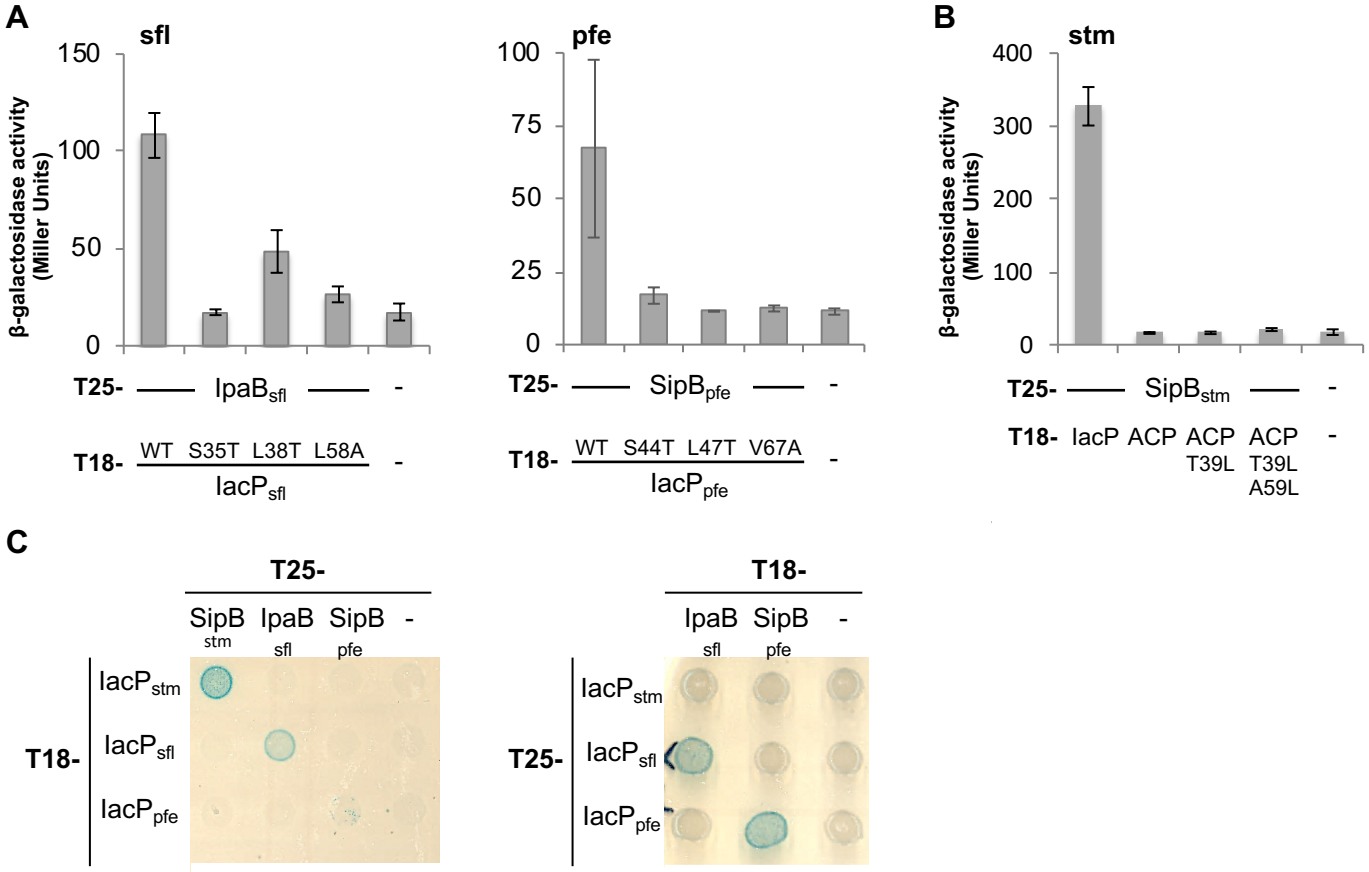


Figure 5. **Interactions between acyl carrier proteins and major hydrophobic translocators associated with SPI-1-like T3SS assayed by the bacterial two-hybrid assays**.

Interactions between pairs of hybrid proteins, resulting from the fusion of the indicated protein with the T18 and T25 fragments of *B. pertussis* adenylated cyclase, were assayed using the bacterial two-hybrid method in *E. coli* BTH101. A positive interaction is indicated by β-galactosidase activity (measured in triplicate, error bars represent the standard error) (A-B) or blue staining on LB agar medium supplemented with IPTG and X-Gal (C). The three-letter code indicates from which organism the genes were cloned: stm for *S.* Typhimurium 12023, sfl for *S. flexneri* M90T, and pfe for *P. fluorescens* F113. A dash indicates the absence of translational fusion with the T18- or T25- fragment. We previously observed that the co-production of the chaperone SicA was necessary to visualize the interaction between IacP and SipB [11]. Therefore, an artificial operon was created on the two-hybrid vector to co-express the hybrid T25- or T18-major hydrophobic translocator with its chaperone (SicA for *S.* Typhimurium, IpgD for *S. flexneri*, and YopD for *P. fluorescens*).

Figure 6

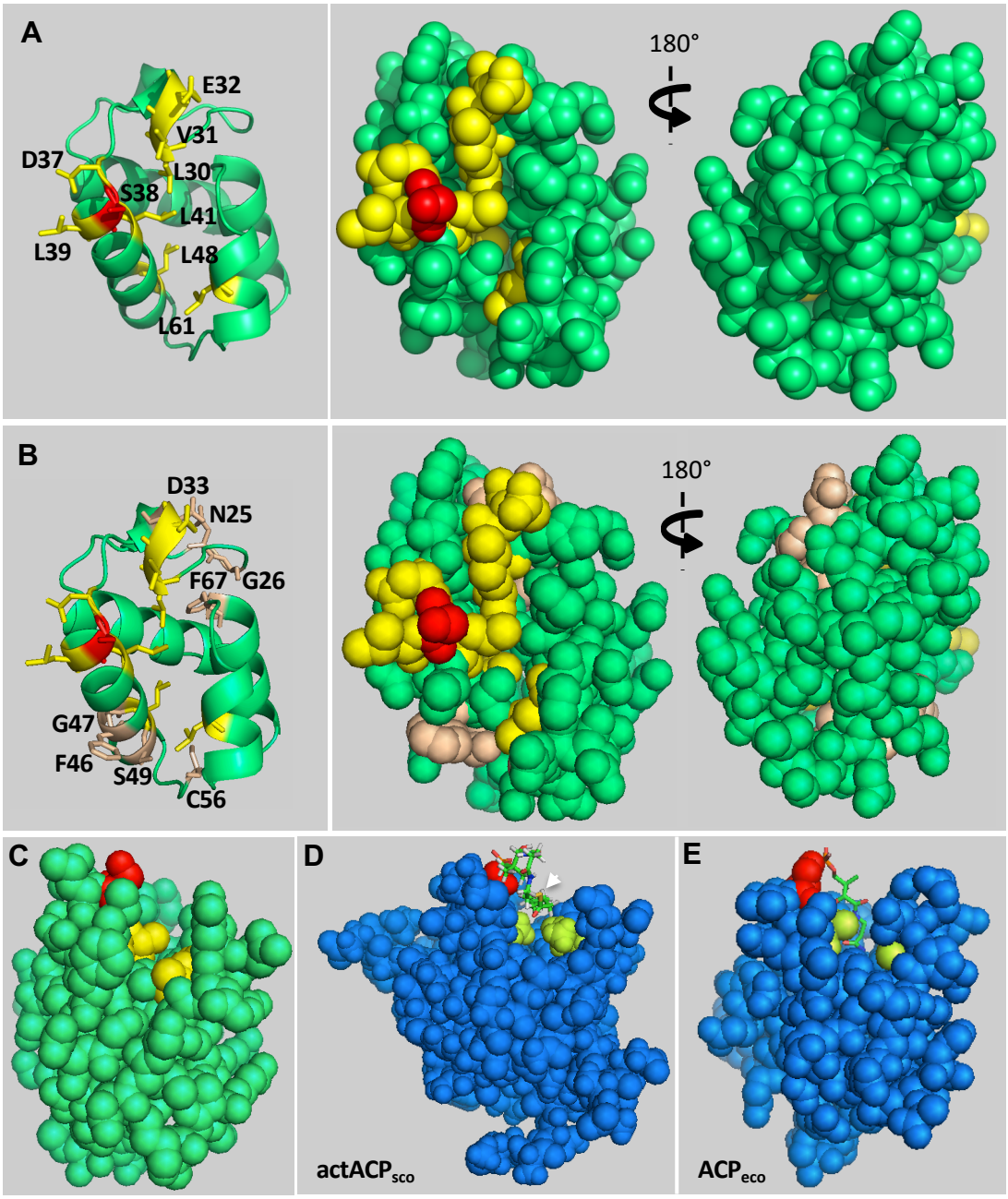


Figure 6. **Location of amino-acid residues of IacP that are involved in the interaction with SipB in a 3D structural model A-B)** The structure of IacP was modeled from *E. coli* ACP, which is involved in fatty acid synthesis (PDB : 1t8k) [38], with which IacP shares 30% identity. The structure of IacP was modeled with a 99.7% confidence score using the intensive modeling mode of the Phyre2 website [39]. Residues that were found to be important for the interaction with SipB by the bacterial two-hybrid method are shown in yellow and the conserved serine residue, which binds 4'-PP, is shown in red (A-B). Residues that were designated to be at the interface of the IacP/SipB complex by the NMR approach, but not found to be necessary for the interaction by the bacterial two-hybrid method, are shown in pale brown (B). Cartoon representation and sphere representation, front and back (rotated 180°, y axis) are shown in the left and right panels, respectively. **C)** Sphere representation of the 3D structural model of IacP. Residues L41 and L61, shown in yellow, are located at the entrance of the hydrophobic cavity. The conserved serine is shown in red. **D-E**) Sphere representation of the 3D structures of the hexanoyl-acyl carrier proteins (blue) involved in the synthesis of the polyketide actinorhodin (actACP$_{sco}$) in *S. coelicolor* (PDB: 2KGA) [27] (D) or fatty acid synthesis in *E. coli* (ACP$_{eco}$) (PDB: 2FAC) [30] (E). The conserved serine is shown in red. Residues found at the corresponding positions of L41 and L61 in IacP are shown in pale green. The hexanoyl-4'-PP, shown as sticks, is exposed to solvent in actACP$_{sco}$, whereas it is inserted and hidden in the hydrophobic cavity of ACP$_{eco}$. The thioester bond (yellow), between the extremity of 4'-PP and the metabolite, is indicated by a white arrowhead in D because it is exposed to solvent and visible, but not in E because it is buried.

Table S1. **List of plasmids**

Unless specified, PCR was performed using *S.* Typhimurium chromosomal DNA as template. The subscripts sfl, pfe, and yen indicate when genomic sequences belong to *S. flexneri, P. fluorescens*, and *Y. enterocolitica*, respectively.

Name	**Lab code**	**Description**	**Reference**
pUT18Clink	pEB355	Amp^R, colE1 ori, P*lac*, T18	[20]
pT18_ACP	pEB379		[20]
pT18_IacP	pJV1		[24]
pT18_IacP-SicA	pJV34		[11]
pT18_$IacP_{NG\ 25\text{-}26\ AA}$-SicA	pJV225	Mutagenesis of pJV34 with primers ebm1681/1682	This study
pT18_$IacP_{L30A}$-SicA	pJV226	Mutagenesis of pJV34 with primers ebm1683/1684	This study
pT18_$IacP_{V31A}$-SicA	pJV252	Mutagenesis ofpJV34 with primers ebm1713/1714	This study
pT18_$IacP_{E32A}$-SicA	pJV166	Mutagenesis of pJV34 with primers ebm1452/1453	This study
pT18_$IacP_{D33A}$-SicA	pJV253	Mutagenesis of pJV34 with primers ebm1715/1716	This study
pT18_$IacP_{D37A}$-SicA	pJV167	Mutagenesis of pJV34 with primers ebm1454/1455	This study
pT18_$IacP_{S38T}$-SicA	pJV168	Mutagenesis of pJV34 with primers ebm798/799	This study
pT18_$IacP_{L39A}$-SicA	pJV227	Mutagenesis of pJV34 with primers ebm1685/1686	This study
pT18_$IacP_{L41T}$-SicA	pJV176	Mutagenesis of pJV34 with primers ebm1492/1493	This study
pT18_$IacP_{L41M}$-SicA	pJV177	Mutagenesis of pJV34 with primers ebm1509/1510	This study
pT18_$IacP_{F46A}$-SicA	pJV228	Mutagenesis of pJV34 with primers ebm1687/1688	This study
pT18_$IacP_{L48A}$-SicA	pJV254	Mutagenesis of pJV34 with primers ebm1717/1718	This study
pT18_$IacP_{S49A}$-SicA	pJV255	Mutagenesis of pJV34 with primers ebm1719/1720	This study
pT18_$IacP_{C56A}$-SicA	pJV114	Mutagenesis of pJV34 with primers ebm1281/1282	This study
pT18_$IacP_{L61A}$-SicA	pJV218	Mutagenesis of pJV34 with primers ebm1662/1663	This study
pT18_$IacP_{F67A}$-SicA	pJV256	Mutagenesis of pJV34 with primers ebm1721/1722	This study
pT18_$IacP_{DI\ 69\text{-}70\ AA}$-SicA	pJV160	Mutagenesis of pJV34 with primers ebm1426/1427	This study
pT18_ACP-SicA	pJV55	PCR with primers ebm1042/1043 cloned into pEB379 at the XhoI site, in the same transcriptional orientation as the T18 fragment	This study
pT18_ACP_{T39L}	pJV180	Mutagenesis of pEB379 with primers ebm1513/1514	This study
pT18_$ACP_{T39L\ A59L}$	pJV221	Mutagenesis of pJV180 with primers ebm1664/1665	This study

pT18_ACP$_{T39L}$-SicA	pJV184	Mutagenesis of pJV55 with primers ebm1513/1514	This study
pT18_IacP$_{sfl}$	pJV137	PCR product with primers ebm1383/1384 on the *S. flexneri* DNA template cloned into pEB355 at the EcoRI/XhoI restriction sites	This study
pT18_IacP$_{sfl}$ S35T	pJV234	Mutagenesis of pJV137 with primers ebm1689/1690	This study
pT18_IacP$_{sfl}$ L38T	pJV193	Mutagenesis of pJV137 with primers ebm1570/1571	This study
pT18_IacP$_{sfl}$ L58A	pJV235	Mutagenesis of pJV137 with primers ebm1707/1708	This study
pT18_IacP$_{pfe}$	pJV196	PCR with primers ebm1586/1587 on the *P. fluorescens* DNA template cloned into pEB355 at the EcoRI/XhoI restriction sites	This study
pT18_AcpY$_{yen}$	pJV204	PCR with primers ebm1611/1612 on the *Y. enterocolitica* DNA template cloned into pEB355 at the EcoRI/XhoI restriction sites	This study
pT18_IpaB$_{sfl}$_IpgC$_{sfl}$	pJV189	PCR with primers ebm1388/1389 and ebm1386/1387 on the *S. flexneri* DNA template cloned into pEB355 at the XbaI/XhoI and XhoI restriction sites, respectively, in the same transcriptional orientation as the T18 fragment	This study
pT18_SipB$_{pfe}$_YopD$_{pfe}$	pJV200	PCR with primers ebm1588/1589 and ebm1590/1591 on the *P. fluorescens* DNA template cloned into pEB355 at the EcoRI/ XhoI and XhoI restriction sites, respectively, in the same transcriptional orientation as the T18 fragment	This study
pT18_YspB$_{yen}$_SycA$_{yen}$	pJV208	PCR with primers ebm1613/1614 and ebm1615/1616 on the *Y. enterocolitica* DNA template cloned into pEB355 at the EcoRI/ XhoI and XhoI restriction sites, respectively, in the same transcriptional orientation as the T18 fragment	This study
pKT25link	pEB354	Kan^R, p15A ori, P*lac*, T25	[20]
pT25_ACP	pEB375		[20]
pT25_IacP	pJV4		[24]
pT25_IacP$_{sfl}$	pJV138	PCR with primers ebm1383/1384 cloned into pEB354 at the EcoRI/ XhoI restriction sites	This study
pT25_IacP$_{pfe}$	pJV197	PCR with primers 1586/1587 cloned into pEB354 at the EcoRI/ XhoI restriction sites	This study

pT25_IacP$_{pfe\ S44T}$	pJV248	Mutagenesis of pJV197 with primers ebm1695/1696	This study
pT25_IacP$_{pfe\ L47T}$	pJV203	Mutagenesis of pJV197 with primers ebm1609/1610	This study
pT25_IacP$_{pfe\ V67A}$	pJV249	Mutagenesis of pJV197 with primers ebm1697/1698	This study
pT25_AcpY$_{yen}$	pJV205	PCR with primers ebm1611/1612 on the *Y. enterocolitica* DNA template cloned into pEB354 at the EcoRI/XhoI restriction sites	This study
pT25_SipB	pJV28		[11]
pT25_SipB-SicA	pJV56		[11]
pT25_IpaB$_{sfl}$-IpgC$_{sfl}$	pJV191	PCR with primers ebm1388/1389 and ebm1386/1387 on the *S. flexneri* DNA template cloned into pEB354 at the XbaI/XhoI and XhoI restriction sites, respectively, in the same transcriptional orientation as the T25 fragment	This study
pT25_SipB$_{pfe}$-YopD$_{pfe}$	pJV201	PCR with primers ebm1588/1589 and ebm1590/1591 on the *P. fluorescens* DNA template cloned into pEB354 at the EcoRI/ XhoI and XhoI restriction sites, respectively, in the same transcriptional orientation as the T25 fragment	This study
pT25_YspB$_{yen}$_SycA$_{yen}$	pJV208	PCR with primers ebm1613/1614 and ebm1615/1616 on the *Y. enterocolitica* DNA template cloned into pEB354 at the EcoRI/ XhoI and XhoI restriction sites, respectively, in the same transcriptional orientation as the T18 fragment	This study
pET$_{6His-TEV-}$	pEB1188	Amp^R, f1 ori, T7 promoter, 6His	[22]
pET$_{6His-TEV-}$IacP	pEB1435	PCR with primers ebm674/675 cloned into pEB1188 at the EcoRI/XhoI restriction sites	This study
pP$_{TET}$	pEB1242	Amp^R, colE1 ori, P$_{TET}$, 6His	pASK-IBA37plus, IBA
pP$_{TET-}$*sipB-sicA*	pJV85		[11]
pP$_{TET-}$*sicA*	pJV101	PCR with primers ebm1041/1043 cloned into pEB1242 at the EcoRI/ XhoI restriction sites	This study
pP$_{TET-}$*iacP*	pJV102		[11]
pP$_{TET-}$*iacP*L30A	pJV297	Mutagenesis of pJV102 with primers ebm1683/1684	This study
pP$_{TET-}$*iacP*V31A	pJV290	Mutagenesis of pJV102 with primers ebm1713/1714	This study
pP$_{TET-}$*iacP*E32A	pJV291	Mutagenesis of pJV102 with primers ebm1452/1453	This study

pP_{TET}-*iacP*D33A	pJV292	Mutagenesis of pJV102 with primers ebm1715/1716	This study
pP_{TET}-*iacP*D37A	pJV296	Mutagenesis of pJV102 with primers ebm1454/1455	This study
pP_{TET}-*iacP*$_{S38T}$	pJV152		[11]
pP_{TET}-*iacP*L41T	pJV188	Mutagenesis of pJV102 with primers ebm1578/1579	This study
pP_{TET}-*iacP*L48A	pJV293	Mutagenesis of pJV102 with primers ebm1717/1718	This study
pP_{TET}-*iacP*L61A	pJV298	Mutagenesis of pJV102 with primers ebm1662/1663	This study

Table S2. **List of primers**

Chromosomal sequences are in upper case, restriction sites are in bold, and ribosome-binding sites are underlined.

Lab code	Purpose	Sequence 5'-3'
ebm674	Cloning *iacP*	tcta**gaattc**ATGaatatggatattgaagcaagagTC
ebm675		ttg**ctcgag**ctacaccctggactcaagac
ebm798	Mutation $IacP_{S38T}$	GATCTTTACGCTGACaCATTGGATTTAATTG
ebm799		CAATTAAATCCAATGtGTCAGCGTAAAGATC
ebm1041	Cloning *sicA*	gaa**gaattc**ATGGATTATCAAAATAATGTCAG
ebm1042		ctc**ctcgag**aaggagatataccATGGATTATCAAAATAATGTCAG
ebm1043		ctc**ctcgag**TTATTCCTTTTCTTGTTCACTG
ebm1281	Mutation $IacP_{C56A}$	GTGAGGAGTTTGACATTAGTgcCAATGAAAACGATCTTCCTGA
ebm1282		TCAGGAAGATCGTTTTCATTGgcACTAATGTCAAACTCCTCAC
ebm1383	Cloning $iacP_{sfl}$	gaa**gaattc**ATGATAAAAGAAAAAATATTATCAATAG
ebm1384		ctc**ctcgag**CTATATTGATTTTGTACTATTTTTG
ebm1386	Cloning $ipgC_{sfl}$	gtc**gtcgac**aaggagatataccATGTCTTTAAATATCACCGAAAATG
ebm1387		gtc**gtcgac**TTACTCCTTGATATCCTGAATTG
ebm1388	Cloning $ipaB_{sfl}$	tct**tctagaattc**ATGCATAATGTAAGCACCACAAC
ebm1389		ctc**ctcgag**TCAAGCAGTAGTTTGTTGCAAAATTG
ebm1452	Mutation $IacP_{E32A}$	CCCATCTGGTTGcGGATCTTTACGC
ebm1453		GCGTAAAGATCCgCAACCAGATGGG
ebm1454	Mutation $IacP_{D37A}$	GATCTTTACGCTGcCTCATTGGATTTA
ebm1455		TAAATCCAATGAGgCAGCGTAAAGATC
ebm1492	Mutation $IacP_{L41T}$	GCTGACTCATTGGATacAATTGATATTG
ebm1493		CAATATCAATTgtATCCAATGAGTCAGC
ebm1509	Mutation $IacP_{L41M}$	CGCTGACTCATTGGATaTgATTGATATTGTATTTG
ebm1510		CAAATACAATATCAATcAtATCCAATGAGTCAGCG
ebm1513	Mutation ACP_{T39L}	GCGGATTCTCTTGACctCGTTGAGCTGGTAATG
ebm1514		CATTACCAGCTCAACGagGTCAAGAGAATCCGC

ebm1570	Mutation $IacP_{sfl\ L38T}$	CGATTCTCTTTCTacGATTGAAATGCTG
ebm1571		CAGCATTTCAATCgtAGAAAGAGAATCG
ebm1578	Mutation $IacP_{L41T}$	CTTTACGCTGACTCATTGGATacAATTGATATTGTATTTGGTC
ebm1579		GACCAAATACAATATCAATTgtATCCAATGAGTCAGCGTAAAG
ebm1586	Cloning $iacP_{Pfe}$	gaa**gaattc**ATGTCAGTAAGTCCAGTTGATCGGC
ebm1587		ctc**ctcgag**TTAAACGTCTCGCACCACTGAATCG
ebm1588	Cloning $sipB_{pfe}$	gaa**gaattc**ATGAGTGAAATCAGAAACACCCCAAG
ebm1589		ctc**ctcgag**TCAAACATGCCGAGCCATTTGCAG
ebm1590	Cloning $yopD_{pfe}$	gtc**gtcgac**aaggagatataccATGGCAGCGTGCCTGTCGGCG
ebm1591		gtc**gtcgac**TCAGTCCTCCGAACAGTGCTGTT
ebm1609	Mutation $IacP_{pfe\ L47T}$	CTGTATATCGATTCCATGGGTacGGTTGAGCTTGTCCTGGAAGTG
ebm1610		CACTTCCAGGACAAGCTCAACCgtACCCATGGAATCGATATACAG
ebm1611	Cloning $acpY_{yen}$	gaa**gaattc**ATGAAACCAGAAAACTCTCAGGAAT
ebm1612		ctc**ctcgag**TCAGTGAGTGATCTCTTCCAAATAA
ebm1613	Cloning $yspB_{yen}$	gaa**gaattc**ATGGTCGATATAAAAGCTGGCAG
ebm1614		ctc**ctcgag**TTAAGCAAAACTGCTTTTTATTATATT
ebm1615	Cloning $SycA_{yen}$	gtc**gtcgac**AAGGAGatataccATGAACCAGAAACATGATGCGGC
ebm1616		gtc**gtcgac**TTATCCTTCTGCTGGTTCACTTTC
ebm1662	Mutation $IacP_{L61A}$	CATTAGTTGCAATGAAAACGATgcTCCTGATATGATGACCTTTGCG
ebm1663		CGCAAAGGTCATCATATCAGGAgcATCGTTTTCATTGCAACTAATG
ebm1664	Mutation ACP_{A59L}	GATACTGAGATTCCGGACGAAGAActTGAGAAAATCACCACCGTTCAG
ebm1665		CTGAACGGTGGTGATTTTCTCAagTTCTTCGTCCGGAATCTCAGTATC
ebm1681	Mutation $IacP_{NG25\text{-}26\ AA}$	CCGTTGATGTTGATAGTATCgcTGcTCAGACCCATCTGGTTGAGG
ebm1682		CCTCAACCAGATGGGTCTGAgCAgcGATACTATCAACATCAACGG
ebm1683	Mutation $IacP_{L30A}$	GTATCAATGGTCAGACCCATgcGGTTGAGGATCTTTACGCTG
ebm1684		CAGCGTAAAGATCCTCAACCgcATGGGTCTGACCATTGATAC
ebm1685	Mutation $IacP_{L39A}$	GGATCTTTACGCTGACTCAgcGGATTTAATTGATATTGTATTTG
ebm1686		CAAATACAATATCAATTAAATCCgcTGAGTCAGCGTAAAGATCC

ebm1687	Mutation $IacP_{F46A}$	GGATTTAATTGATATTGTAgcTGGTCTTAGTGAGGAGTTTG
ebm1688		CAAACTCCTCACTAAGACCAgcTACAATATCAATTAAATCC
ebm1689	Mutation $IacP_{sfl\ S35T}$	TATTGAAGATCTTTCTGCCGATaCTCTTTCTCTGATTGAAATGCTG
ebm1690		CAGCATTTCAATCAGAGAAAGAGtATCGGCAGAAAGATCTTCAATA
ebm1695	Mutation $IacP_{pfe\ S44T}$	GTCGAGGACCTGTATATCGATaCCATGGGTTTGGTTGAGCTTG
ebm1696		CAAGCTCAACCAAACCCATGGtATCGATATACAGGTCCTCGAC
ebm1697	Mutation $IacP_{pfe\ V67A}$	GAATTGTCTGAAGATGAGGcGGGGGAGTGGCGGACGGTGCAG
ebm1698		CTGCACCGTCCGCCACTCCCCCgCCTCATCTTCAGACAATTC
ebm1707	Mutation $IacP_{sfl\ L58A}$	CGTATAGATGAATCTGCAgcAGAACACATTATTACTATTGG
ebm1708		CCAATAGTAATAATGTGTTCTgcTGCAGATTCATCTATACG
ebm1713	Mutation $IacP_{V31A}$	CAATGGTCAGACCCATCTGGcTGAGGATCTTTACGCTGACTC
ebm1714		GAGTCAGCGTAAAGATCCTCAgCCAGATGGGTCTGACCATTG
ebm1715	Mutation $IacP_{D33A}$	GTCAGACCCATCTGGTTGAGGcTCTTTACGCTGACTCATTGG
Ebm1716		CCAATGAGTCAGCGTAAAGAgCCTCAACCAGATGGGTCTGAC
ebm1717	Mutation $IacP_{L48A}$	TAATTGATATTGTATTTGGTgcTAGTGAGGAGTTTGACATTAG
ebm1718		CTAATGTCAAACTCCTCACTAgcACCAAATACAATATCAATTA
ebm1719	Mutation $IacP_{S49A}$	GATATTGTATTTGGTCTTgcTGAGGAGTTTGACATTAGTTGC
ebm1720		GCAACTAATGTCAAACTCCTCAgcAAGACCAAATACAATATC
ebm1721	Mutation $IacP_{F67A}$	CTTCCTGATATGATGACCgcTGCGGATATATGCCGTGTTG
ebm1722		CAACACGGCATATATCCGCAgcGGTCATCATATCAGGAAG

SUPPLEMENTAL FIGURE LEGENDS

Figure S1. **Production of T18-acyl carrier hybrid proteins**

Western blots were performed on whole-cell extracts of *E. coli* DH5α transformed with plasmids allowing production of the mentioned T18-hybrid protein (A., first and second panels, and B.) or on whole-cell extracts of *E. coli* DH5α co-transformed with plasmids allowing both production of the T18- hybrid protein and the T25-$SipB_{stm}$ hybrid protein (A. third panel). The antibody was directed against the T18 domain of the *B. pertussis* adenylate cyclase. The migration of ACPs may depend on whether the proteins are in the apo-, holo-, or acylated-form and whether they have substituted amino acids [13, 24, 31, 40, 41]. The quality of the antibody directed against the T25 fragment of the adenylate cyclase and the level of expression from this low-copy two-hybrid plasmid did not allow the detection of any T25 hybrid proteins.

Figure S2. **Complementation test of *E. coli* ACP^{ts} mutant strain with ACP_{T39L}**

E. coli ACP^{ts} was transformed with the plasmids used for the bacterial two-hybrid experiments pT18-ACP_{T39L}, pT18-ACP, and pT18 and grown for three days at 30°C or 42°C. Although all strains were able to grow at 30°C, only the ACP^{ts} strain complemented by pT18-ACP was able to grow at 42°C.

Figure S1

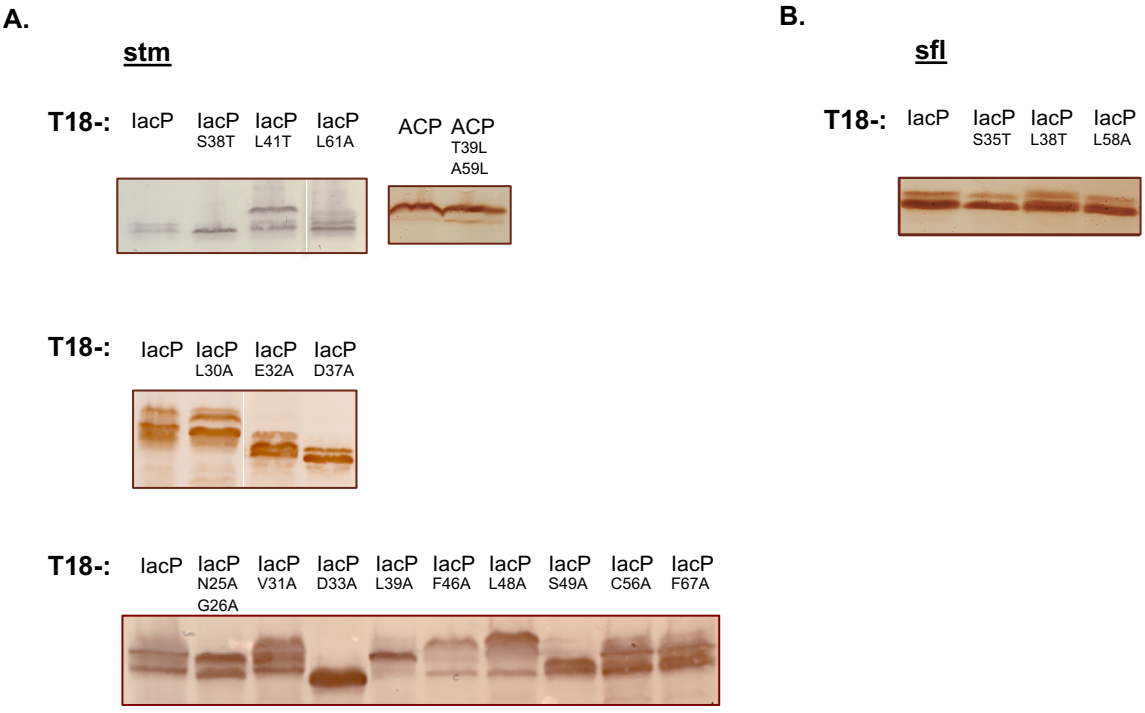


Figure S1. **Production of T18-acyl carrier hybrid proteins**
Western blots were performed on whole-cell extracts of *E. coli* DH5α transformed with plasmids allowing production of the mentioned T18-hybrid protein (A., first and second panels, and B.) or on whole-cell extracts of *E. coli* DH5a co-transformed with plasmids allowing both production of the T18- hybrid protein and the T25-$SipB_{stm}$ hybrid protein (A. third panel). The antibody was directed against the T18 domain of the *B. pertussis* adenylate cyclase. The migration of acyl carrier proteins may depend on whether the proteins are in the apo-, holo-, or acylated-form and whether they have substituted amino acids [13,19,24,39,40]. The quality of the antibody directed against the T25 fragment of the adenylate cyclase and the level of expression from this low-copy two-hybrid plasmid did not allow the detection of any T25 hybrid proteins.

Figure S2

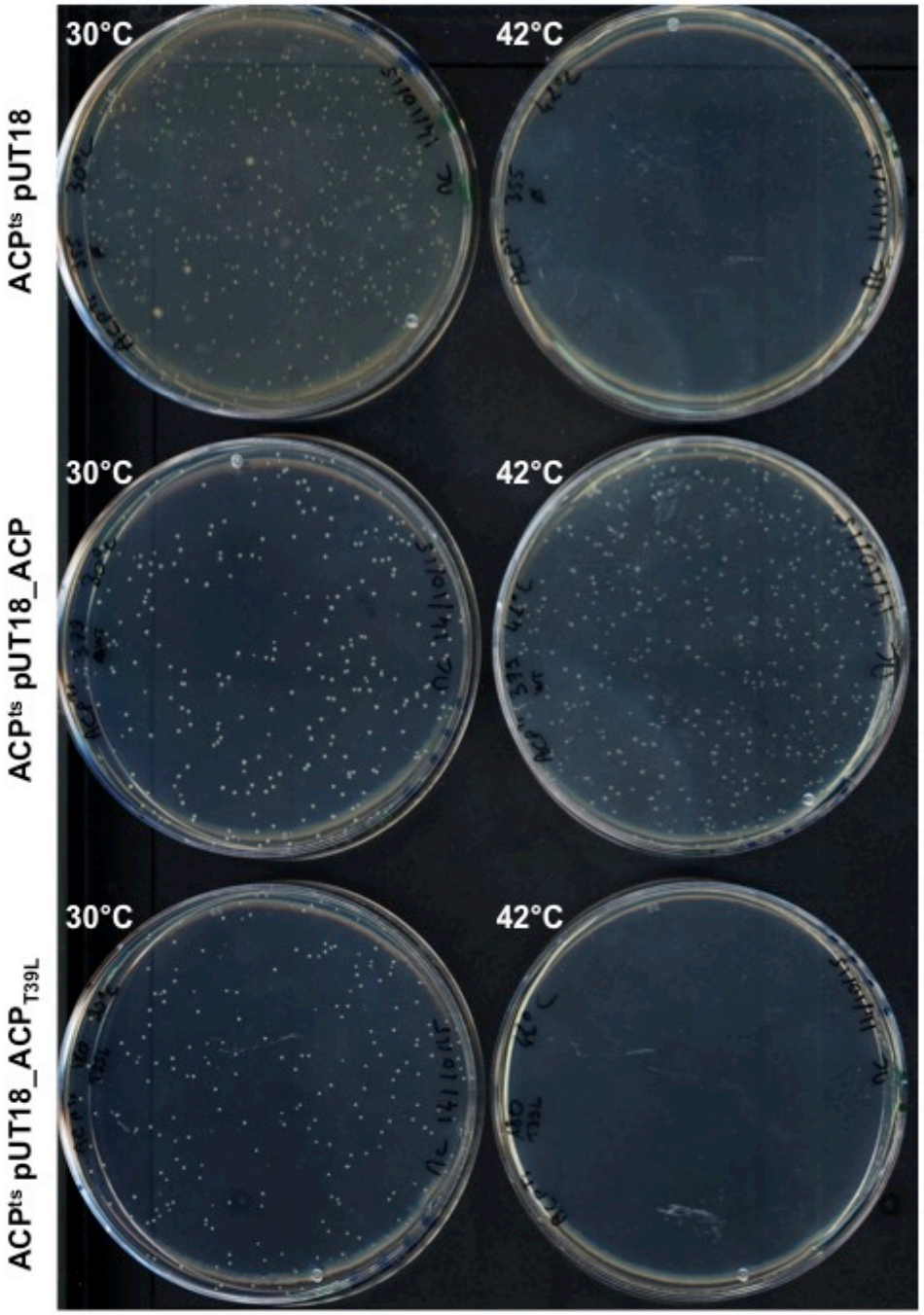


Figure S2. **Complementation test of *E. coli* ACP^{ts} mutant strain with ACP$_{T39L}$**
E. coli ACP^{ts} was transformed with the plasmids used for the bacterial two-hybrid experiments pT18-ACP$_{T39L}$, pT18-ACP, and pT18 and was grown for three days at 30°C or 42°C. Although all strains were able to grow at 30°C, only the ACP^{ts} strain complemented by pT18-ACP was able to grow at 42°C.